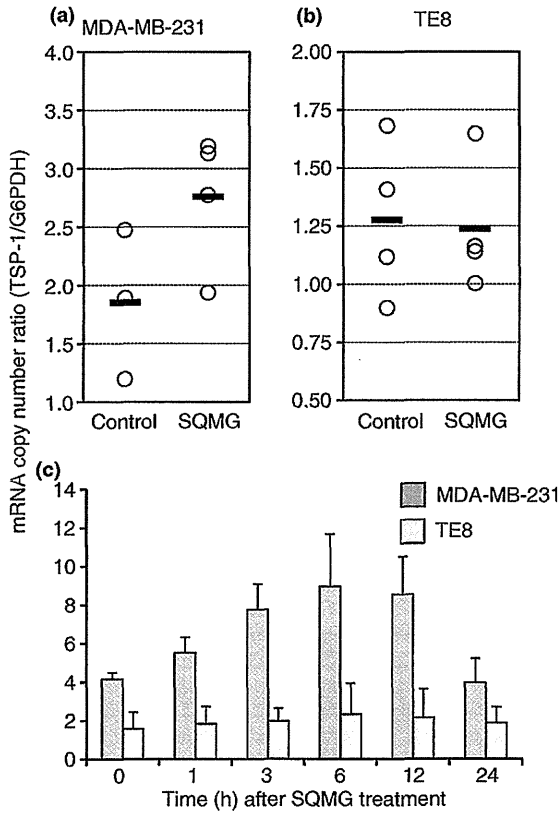

Fig. 2. Upregulation of *thrombospondin 1 (TSP-1)* gene expression by 3′-sulfoquinovosyl-1′-monoacylglycerol (SQMG) in MDA-MB-231 cells. *TSP-1* mRNA copy number in xenografted tumors derived from MDA-MB-231 (a) or TE-8 (b) treated with or without SQMG *in vivo* were measured by quantitative real time polymerase chain reaction (PCR). Data are presented as *TSP-1* mRNA copy number per the copy number of *G6PDH* indicating by open circles. Bar indicates means of each test group. (c) The means ± standard error (SE) of *TSP-1* mRNA copy numbers of MDA-MB-231 (dark gray bar) or TE-8 (light gray bar) treated with 25 μM SQMG *in vitro* are presented, which normalized with the mRNA copy number of *G6PDH*.

TSP-1-overexpressing transformants were unable to grow *in vivo*. In order to confirm the anti-angiogenic effects of TSP-1, SQMG-resistant TE-8 cells were transfected with *TSP-1* cDNA and TSP-1-overexpressing transformants (TSP1-OT) were cloned. We selected three clones (i.e., clones 4, 8 and 13) that showed approximately threefold expression of *TSP-1*, as compared with intact TE-8 or empty vector (pcDNA3.1) control (Fig. 3a). These three TSP1-OT clones had similar growth rates *in vitro* when compared with controls (Fig. 3b). However, the TSP1-OT clone cells (TSP1-OT clone 4) did not grow *in vivo* (Fig. 3c). Implantation using other clones, such as clones 8 and 13, was also attempted; however, growth of these clones *in vivo* was not observed. These data suggest that overexpression of TSP-1 is critical for tumorigenesis.

Establishment and characterization of stable TSP-1-knockdown transformant. We designed five shRNAs and used the Mission *RNAi* (Sigma-Aldrich) technology platform to stably knockdown *TSP-1* gene expression in SQMG-sensitive MDA-MB-231 cells. When sh-2 shRNA was transfected into the cells, the endogenous *TSP-1* gene expression decreased by approximately 92%, as compared with the sh-control treated with shRNA for a non-target gene (Fig. 4a). Among the five shRNAs, sh-2 most effectively induced the downregulation of TSP-1 expression. Using the sh-2 transformants, we successfully obtained a stable TSP-1 knockdown transformant clone, clone 80 (TSP1-KT), which showed approximately 94% reduced *TSP-1* gene expression when compared with the sh-control (Fig. 4b). We further investigated the growth rate of TSP1-KT (clone 80) *in vitro* using MTT assay. No differences in growth rates were observed between TSP1-KT and the sh-control was observed, thus suggesting that TSP-1 did not influence *in vitro* growth activity (Fig. 4c).

To investigate the mechanism of TSP-1 upregulation by SQMG, we performed Dual-Luciferase reporter assay. If SQMG stimulation is transduced via TSP-1 molecules to induce TSP-1 expression, TSP1-KT would have no effect. As cDNA encoding TSP-1-targeting sh-RNA is stably expressed in TSP1-KT, we were unable to detect TSP-1 gene expression. Therefore, to investigate this signal transduction, we used a Dual-Luciferase reporter assay using the TSP-1 promoter that would not influence the sh-RNA system.[16] When sh-control cells were introduced with luciferase reporter constructs containing the TSP-1-promoter, luciferase expression of SQMG-treated cells was significantly increased from 1 to 3 h after treatment as compared with non-treatment control ($P < 0.05$, Fig. 4d). These data demonstrate that SQMG is able to induce *TSP-1* gene expression, which supports the real-time PCR data shown in Fig. 2c, although a time lag was observed. On the other hand, when TSP1-KT was introduced with luciferase reporter constructs with culture in the presence or absence of SQMG, no differences were observed, thus suggesting that TSP-1 upregulation by SQMG occur via TSP-1 molecule (Fig. 4e).

The tumorigenic potential of TSP1-KT *in vivo* was then investigated by subcutaneously injecting them into mice, and mice bearing solid tumors that grew to 30–40 mm^3 in volume were then injected intraperitoneally with saline or SQMG daily for 14 days (days 16–30). As shown in Figure 4(f), SQMG treatment of mice bearing sh-control solid tumors resulted in significant inhibition of tumor growth when compared with the saline-treated control group ($P < 0.05$). In contrast, SQMG treatment of mice bearing TSP1-KT solid tumors did not lead to tumor growth inhibition, as compared with the control group (Fig. 4g). These data confirm that growth of TSP1-KT solid tumors is not inhibited by SQMG treatment, thus suggesting that anti-angiogenesis via TSP-1 upregulation induced by SQMG treatment did not occur, as the SQMG target molecule TSP-1 was knocked down in TSP1-KT transformants.

In accordance with our previous study, we further performed immunohistochemical analysis to determine the angiogenesis profiles of tumors in an effort to confirm the absence of anti-tumor effects by SQMG treatment in TSP1-KT tumors.[15] Tumors were excised from the mice and cryosections of the acetone-fixed tumors were stained with anti-mouse CD31 mAb as an endothelial cell marker. Representative photographs showing immunohistochemical staining of tumors treated with or without SQMG are shown in Figure 5. CD31-positive/ring-form blood vessels were clearly observed for both the sh-control (Fig. 5a,b) and TSP1-KT (Fig. 5c,d), and were counted for all samples in 500-mm^2 section areas under a fluorescence microscope. As shown in Figure 5(e), the number of blood vessels was significantly higher ($P < 0.01$) in TSP1-KT control tumors when compared with sh-control control tumors, thus suggesting that the downregulation of TSP-1 facilitated more angiogenesis. In contrast, in TSP1-KT tumors treated with or without SQMG, no significant differences in the number of blood vessels were observed. However, the number of blood vessels in the sh-control tumors was significantly lower ($P < 0.05$) after SQMG treatment when compared with TSP1-KT tumors.

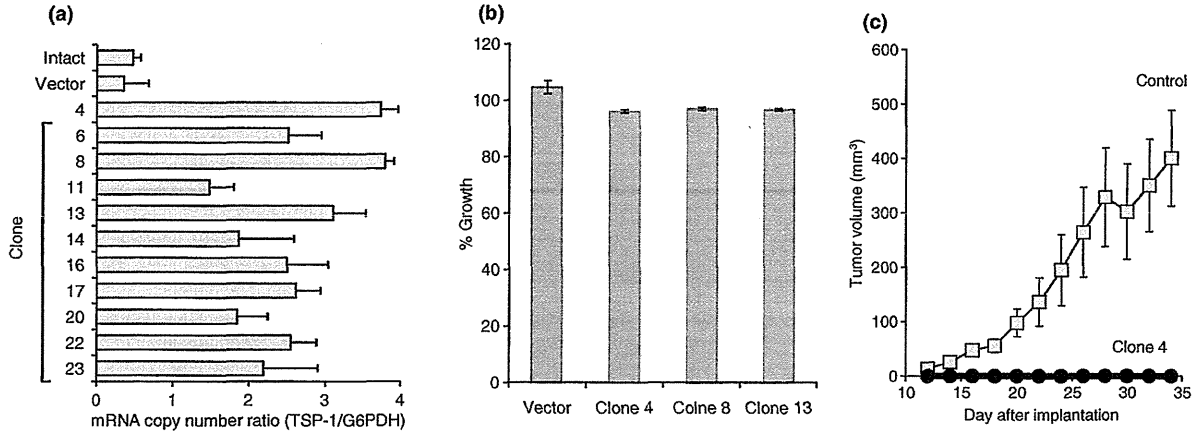

Fig. 3. Establishment of thrombospondin 1 (TSP-1)-overexpressed transformant (TSP1-OT) and the assessment of tumorigenesis *in vivo*. TE-8 cells were transfected with TSP-1 cDNA in pcDNA3.1 vector or empty vector, and selected, cloned, and established several clones (TSP1-OT). (a) TSP-1 mRNA copy number of TSP-1-overexpressed transformants were measured by real time polymerase chain reaction (PCR). (b) Growth rate of three TSP1-OT clones *in vitro* were measured by 3-(4,5-dimethylthiazol-2-yl)-2,5-diphenyltetrazolium bromide (MTT) assay. (c) 10^6 TSP1-OT clone 4 or control cells were subcutaneously injected into mice and the tumor sizes were measured at 2-day intervals in each mouse. The means ± standard error (SE) of tumor volumes from each group (n = 4/group) are shown.

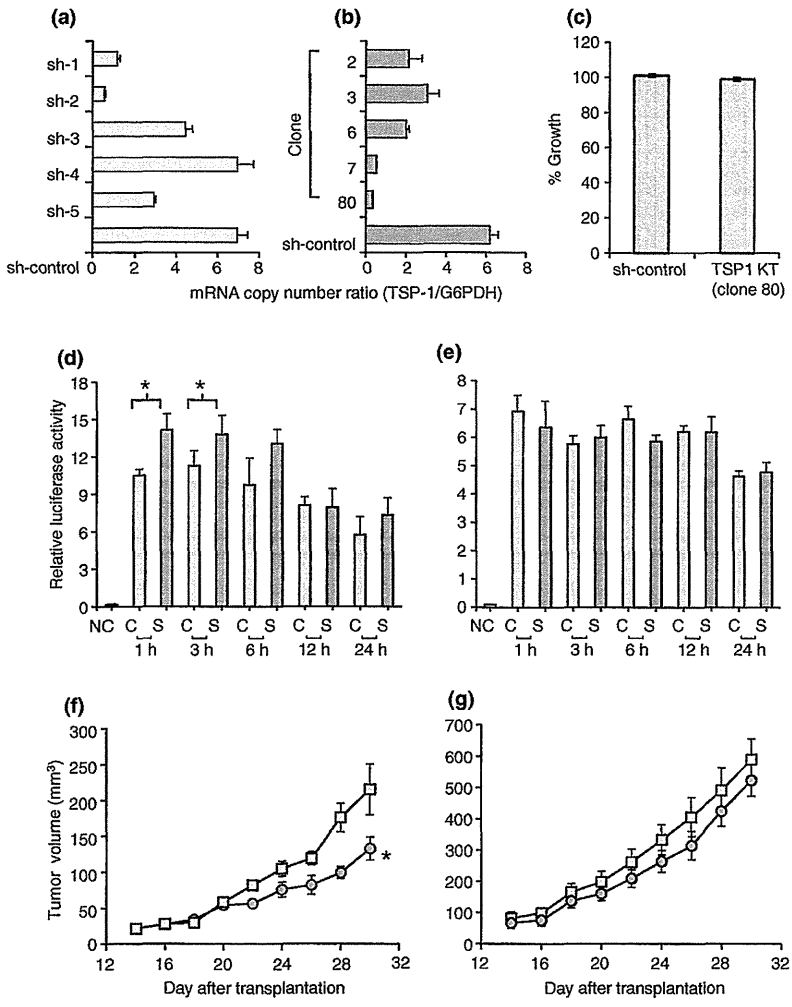

Fig. 4. Establishment of thrombospondin 1 (TSP-1)-knockdown transformant clone (TSP1-KT) and the assessment of tumorigenesis *in vivo*. (a) Plasmid DNA including five TSP-1-targeting (sh1–5) or non-targeting shRNAs (sh-control) ligated into pLKO.1-puro shRNA vector were transfected into MDA-MB-231 cells along with Lentiviral Packaging Mix. TSP-1 mRNA copy number of these TSP1-KT clones were measured by real time polymerase chain reaction (PCR). (b) MDA-MB-231 cells were introduced sh-2 shRNA, and selected, cloned, and TSP-1 mRNA copy number of these cells was measured by real time PCR. (c) Growth rate of TSP1-KT clone (clone 80) *in vitro* were measured by by 3-(4,5-dimethylthiazol-2-yl)-2,5-diphenyltetrazolium bromide (MTT) assay. (d and e) Data of reporter assay using TSP-1 promoter. sh-control (d) and TSP1-KT (e) cells were transfected with reporter plasmids together with pGL4.74 plasmid as an internal control and then cultured with or without 3′-sulfoquinovosyl-1′-monoacylglycerol (SQMG) representing S or C, respectively. The relative luciferase activity for each cell was calculated relative to the activity of the promoterless plasmid (negative control representing NC). Data are the means ± standard error (SE) (n = 3 in three trials; $^*P < 0.05$). (f and g) *In vivo* assessment of anti-tumor effects of SQMG using TSP1-KT. 10^6 TSP1-KT (g) or control cells (f) were subcutaneously injected into mice. When the solid tumors grew to 30–40 mm^3 in tumor volume, mice were injected with SQMG at a dose of 20 mg/kg (SQMG 20) or saline (control) daily for 14 days. The means ± SE of tumor volumes from each group (n = 4/group) are shown. $^*P < 0.01$.

doi: 10.1111/j.1349-7006.2012.02333.x

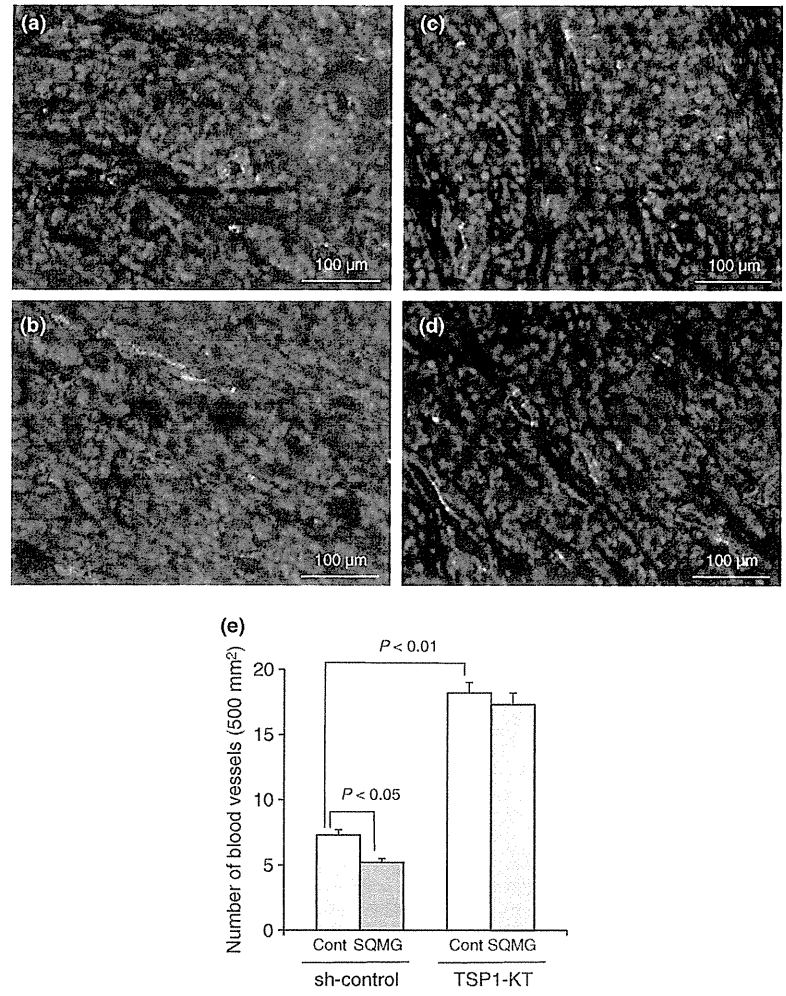

Fig. 5. Assessment of antiangiogenesis by immunohistochemical staining. Cryosections of sh-control tumors treated with (a) and without (b) 3′-sulfoquinovosyl-1′-monoacylglycerol (SQMG) were stained by anti-mouse CD31 mAb/anti-rat IgG conjugated with AlexaFlour 488, and nuclei were counterstained with PI. TSP1-KT tumors treated with (c) and without (d) SQMG were stained by anti-mouse CD31 mAb/anti-rat IgG conjugated with AlexaFlour 488, and nuclei were counterstained with propidium iodide. Arrows indicate CD31-positive blood vessels. Scale bar = 100 μm.

Discussion

In this study, we showed that SQMG is not anti-angiogenic in TSP-1-knockdown xenograft tumors, thus suggesting that the anti-tumor effects of SQMG can be attributed to the inhibition of tumor angiogenesis via the upregulation of TSP-1. TSP-1 is an oligomeric extracelluar matrix glycoprotein that mediates cell–cell and cell–matrix interactions by binding to cell-surface receptors, such as CD36 and integrin-associated protein (IAP)/CD47.[9,17–19] Several mechanisms have been reported to explain the anti-angiogenic effects of TSP-1 including endothelial cell apoptosis.[7–9,20] The association between TSP-1 and CD36, which is known to be expressed on endothelial cells and is a receptor for TSP-1, induces endothelial cell apoptosis through the sequential activation of Fyn phosphorylation, caspase-3-like proteases and p38 MAPK activity.[9,21] Thrombospondin 1 has also been reported to have an effect on VEGF-A-induced phosphorylation of VEGFR2 via the activation of CD36, which induces the inhibition of endothelial migration.[22] Moreover, in the absence of TSP-1, the association of VEGFR-2 with CD36 and spleen tyrosine kinase (Syk) decreased and Syk promoted VEGF-A-induced endothelial cell activity via VEGFR-2 phosphorylation.[23] The association between TSP-1 and CD36 is a major pathway in the inhibition of angiogenesis and ligation of CD47 is reported to inhibit nitric oxide-stimulated angiogenesis and VEGFR2 activation.[18,24] Thus, TSP-1 possesses anti-angiogenic activity, and its upregulation by SQMG results in significant antitumor activity, although these effects depend on the cellular context.

Whether a tumor is sensitive or resistant to SQMG may depend on whether TSP-1 is upregulated in that tumor. To address the mechanism of how TSP-1 is upregulated by SQMG treatment, we investigated the amount of TSP-1 mRNA by real-time PCR and the transcriptional mechanism on the TSP-1 promoter by luciferase reporter assay *in vitro*. Although the mechanism of TSP-1-upregulation by SQMG in xenografted solid tumor *in vivo* has not been fully demonstrated, the presented data suggested that the TSP-1-upregulation by SQMG is necessary for the existence of a signal transduction pathway via TSP-1 molecule. The master regulator of TSP-1 gene expression is known to be p53.[25] Gene expression under the regulation of p53 involves multiple mechanisms, such as post-translational modifications and the availability of transcriptional cofactors that can regulate the activity of p53.[25–27] Indeed, regulation of TSP-1 by p53 appears to vary in different cell and tissue types: for example, TSP-1 expression is correlated with p53 status in prostate cancer,[28,29] liver,[30] ovarian carcinoma[31] and glioma,[32] but is inversely correlated with p53 status in colon cancer.[33] These data suggest that the regulation of TSP-1 expression by p53 is cell context-dependent and that the expression of different p53-binding cofactors may

modulate this regulation. In addition to several transcriptional cofactors, post-transcriptional microRNA (miRNA)-based mechanisms involved in the regulation of TSP-1 were also recently reported. cMyc-activated miR-17-92 was shown to be involved in the downregulation of TSP-1,[34] and p53-activated miR-194 was found to inhibit TSP-1 and promote angiogenesis in colon cancer.[35] This study did not elucidate whether the difference in sensitivity to SQMG was correlated with the cell context-dependent regulation of TSP-1 expression by p53.

We previously reported that significant downregulation of *Tie2* gene expression in endothelial/pericyte cells was observed in all SQMG-sensitive tumors when compared with controls.[16] Results from this study suggest that the anti-tumor effects of SQMG are attributed to the inhibition of tumor angiogenesis via upregulation of TSP-1. It is assumed that TSP-1 upregulation in tumor cells causes Tie2 downregulation in endothelial/pericyte cells, given that SQMG is not anti-angiogenic in the TSP-1 knockdown xenograft tumors. Although little is known about TSP-1-inducible chemical compounds, such a trichostatin A, SQMG is a promising candidate for the treatment of tumor-induced angiogenesis via TSP-1 upregulation.[36]

Acknowledgments

This research was supported by The Special Coordination Funds on Science and Technology of the Ministry of Education, Culture, Sports, Science of Japan and a research project grant awarded by the Azabu University.

Disclosure Statement

The authors have no conflicts of interest.

References

1 Folkman J. What is the evidence that tumor are angiogenesis dependent? *J Natl Cancer Inst* 1990; **82**: 4–6.
2 Carmeliet P. Angiogenesis in life, disease and medicine. *Nature* 2005; **438**: 932–6.
3 Hicklin DJ, Ellis LM. Role of the vascular endothelial growth factor pathway in tumor growth and angiogenesis. *J Clin Oncol* 2005; **23**: 1011–27.
4 Carmeliet P, Jain RK. Molecular mechanisms and clinical applications of angiogenesis. *Nature* 2011; **473**: 298–307.
5 Hurwitz H, Feherenbacher L, Novotny W *et al.* Bevacizumab plus irinotecan, fluorouracil, and leucovorin for metastatic colorectal cancer. *N Engl J Med* 2004; **350**: 2335–42.
6 Ferrara N, Kerbel RS. Angiogenesis as a therapeutic target. *Nature* 2005; **438**: 967–74.
7 Bagvandoss P, Wilks JW. Specific inhibition of endothelial cell proliferation by thrombospondin. *Biochem Biophys Res Commun* 1990; **170**: 867–72.
8 Good DJ, Polverini PJ, Rastinejad F *et al.* A tumor suppressor-dependent inhibitor of angiogenesis is immunologically functionally indistinguishable from a fragment of thrombospondin. *Proc Natl Acad Sci USA* 1990; **87**: 6624–8.
9 Dawson DW, Pearce SF, Zhong R, Silverstein RL, Frazier WA, Bouck NP. CD36 mediates the *in vitro* inhibitory effects of thrombospondin-1 on endothelial cells. *J Cell Biol* 1997; **138**: 707–17.
10 Zang X, Kazerounian S, Duquette M *et al.* Thrombospondin-1 modulated vascular endothelial growth factor activity at the receptor level. *FASEB J* 2009; **23**: 3368–76.
11 Kaur S, Martin-Manso G, Pendrak ML, Garfield SH, Isenberg JS, Robert DD. Thrombospondin-1 inhibit VEGF receptor-2 signaling by disrupting its association with CD47. *J Biol Chem* 2010; **285**: 38923–32.
12 Gupta K, Gupta P, Wild R, Ramakrishnan S, Hebbel RP. Binding and displacement of vascular endothelial growth factor (VEGF) by thrombospondin: effect on human microvascular endothelial cell proliferation and angiogenesis. *Angiogenesis* 1999; **3**: 147–58.
13 Sahara H, Ishikawa M, Takahashi N *et al. In vivo* anti-tumour effect of 3′-sulphonoquinovosyl 1′-monoacylglyceride isolated from sea urchin (*Strongylocentrotus intermedius*) intestine. *Br J Cancer* 1997; **75**: 324–32.
14 Sahara H, Hanashima S, Yamazaki T *et al.* Anti-tumor effect of chemically synthesized sulfolipids based on sea urchin's natural sulfonoquinovosylmonoacylglycerols. *Jpn J Cancer Res* 2002; **93**: 85–92.
15 Mori Y, Sahara H, Matsumoto K *et al.* Downregulation of *Tie2* gene by a novel antitumor sulfolipid, 3′-sulfoquinovosyl-1′-monoacylglycerol (SQMG), targeting angiogenesis. *Cancer Sci* 2008; **99**: 1063–70.
16 Donoviel DB, Framson P, Eldrige CF, Cooke M, Kobayashi S, Bornstein P. Structural analysis and expression of the human thrombospondin gene promoter. *J Biol Chem* 1988; **263**: 18590–3.
17 Isenberg JS, Jia Y, Fukuyama J Switzer CH, Wink DA, Roberts DD. Thrombospondin-1 inhibits nitric oxide signaling via CD36 by inhibiting myristic acid uptake. *J Biol Chem* 2007; **282**: 15404–15.
18 Isenberg JS, Ridnour LA, Dimitry J *et al.* CD47 is necessary for inhibition of nitric oxide-stimulated vascular cell responses by thrombospondin-1. *J Biol Chem* 2006; **281**: 26069–80.
19 Krutzsch HC, Choe BJ, Sipes JM, Guo N, Roberts DD. Identification of an alpha(3)beta(1) integrin recognition sequence in thrombospondin-1. *J Biol Chem* 1999; **274**: 24080–6.
20 Isenberg JS, Martin-Manson G, Maxhimer JB, Roberts DD. Regulation of nitric oxide signalling by thrombospondin 1: implications for anti-angiogenic therapies. *Nat Rev Cancer* 2009; **9**: 182–94.
21 Jiménez B, Volpert OV, Crawford SE, Febbraio M, Silverstein RL, Bouck N. Signals leading to apoptosis-dependent inhibition of neovascularization by thrombospondin-1. *Nat Med* 2000; **6**: 41–8.
22 Primo L, Ferrandi C, Roca C *et al.* Identification of CD36 molecular features required for its *in vitro* angiostatic activity. *FASEB J* 2005; **19**: 1713–5.
23 Kazerounian S, Duquette M, Reyes MA *et al.* Priming of the vascular endothelial growth factor signaling pathway by thrombospondin-1, CD36, and spleen tyrosine kinase. *Blood* 2011; **117**: 4658–66.
24 Kaur S, Martin-Manso G, Pendrak ML, Garfield SH, Isenberg JS, Roberts DD. Thrombospondin-1 inhibits VEGF receptor-2 signaling by disrupting its association with CD47. *J Biol Chem* 2010; **285**: 38923–32.
25 Dameron KM, Volpert OV, Tainsky MA, Bouck N. Control of angiogenesis in fibroblasts by p53 regulation of thrombospondin-1. *Science* 1994; **265**: 1582–4.
26 Shinobu N, Maeda T, Aso T *et al.* Physical interaction and functional antagonism between the RNA polymerase II elongation factor ELL and p53. *J Biol Chem* 1999; **274**: 17003–10.
27 Roe JS, Kim H, Lee SM, Kim ST, Cho EJ, Youn HD. p53 stabilization and transactivation by a von Hippel-Lindau protein. *Mol Cell* 2006; **22**: 395–405.
28 Xiao W, Zhang Q, Jiang F, Pins M, Kozlowski JM, Wang Z. Suppression of prostate tumor growth by U19, a novel testosterone-regulated apoptosis inducer. *Cancer Res* 2003; **63**: 4698–704.
29 Kwak C, Jin RJ, Lee C, Park MS, Lee SE. Thrombospondin-1, vascular endothelial growth factor expression and their relationship with p53 status in prostate cancer and benign prostatic hyperplasia. *BJU Int* 2002; **89**: 303–9.
30 Su F, Pascal LE, Xiao W, Wang Z. Tumor suppressor U19/EAF2 regulates thrombospondin-1 expression via p53. *Oncogene* 2010; **29**: 421–31.
31 Alvarez AA, Axelrod JR, Whitaker RS *et al.* Thrombospondin-1 expression in epithelial ovarian carcinoma: association with p53 status, tumor angiogenesis, and survival in platinum-treated patients. *Gynecol Oncol* 2001; **82**: 273–8.
32 Harada H, Nakagawa K, Saito M *et al.* Introduction of wild-type p53 enhances thrombospondin-1 expression in human glioma cells. *Cancer Lett* 2003; **191**: 109–19.
33 Tokunaga T, Nakamura M, Oshika Y *et al.* Alterations in tumour suppressor gene p53 correlate with inhibition of thrombospondin-1 gene expression in colon cancer cells. *Virchows Arch* 1998; **433**: 415–8.
34 Dews M, Homayouni A, Yu D *et al.* Augmentation of tumor angiogenesis by a myc-activated microRNA cluster. *Nat Genet* 2006; **38**: 1060–5.
35 Sundaram P, Hultine S, Smith LM *et al.* p53-responsive miR-194 inhibits thrombospondin-1 and promotes angiogenesis in colon cancers. *Cancer Res* 2011; **71**: 7490–501.
36 Kang JH, Kim SA, Chang SY, Hong S, Hong KJ. Inhibition of trichostatin A-induced antiangiogenesis by small-interfering RNA for thrombospondin-1. *Exp Mol Med* 2007; **39**: 402–11.

doi: 10.1111/j.1349-7006.2012.02333.x

Carcinogenesis vol.33 no.5 pp.996–1003, 2012
doi:10.1093/carcin/bgs118
Advance Access publication March 12, 2012

ECRG4 is a negative regulator of caspase-8-mediated apoptosis in human T-leukemia cells

Junichi Matsuzaki, Toshihiko Torigoe*, Yoshihiko Hirohashi, Kenjiro Kamiguchi, Yasuaki Tamura, Tomohide Tsukahara, Terufumi Kubo, Akari Takahashi[1], Emiri Nakazawa[1], Eri Saka, Kazuyo Yasuda, Shuji Takahashi and Noriyuki Sato

Department of Pathology, Sapporo Medical University School of Medicine, South-1 West-17, Chuo-ku, Sapporo 060-8556, Japan and [1]Japan Science and Technology Corporation, Innovation Plaza Hokkaido, Sapporo 060-0819, Japan

*To whom correspondence should be addressed. Tel: +81 11 613 8374; Fax: +81 11 643 2310;
Email: torigoe@sapmed.ac.jp

We previously established Fas-resistant variant clones from the human T-cell leukemia lines Jurkat and SUP-T13. Comparative gene expression analysis of the Fas-resistant and Fas-sensitive clones revealed several genes that were aberrantly expressed in the Fas-resistant clones. One of the genes, esophageal cancer-related gene 4 (*ECRG4*), contained a VDAC2-like domain that might be associated with apoptotic signals. In the present study, we examined the subcellular localization and function of ECRG4 in Fas-mediated apoptosis. By confocal fluorescence microscopy, ECRG4-EGFP fusion protein was detected in mitochondria, endoplasmic reticulum and the Golgi apparatus in gene-transfected HeLa cells. Overexpression of ECRG4 in Fas-sensitive Jurkat cells inhibited mitochondrial membrane permeability transition, leading to resistance against Fas-induced apoptosis. Tumor necrosis factor-alpha-induced apoptosis was also suppressed in ECRG4-overexpressing Jurkat cells. Immunoprecipitation assay demonstrated that ECRG4 is associated with procaspase-8. The inhibitory mechanism included the inhibition of caspase-8 activity and Bid cleavage. Since ECRG4 expression is downregulated in activated T cells, our results suggest that ECRG4 is a novel antiapoptotic gene which is involved in the negative regulation of caspase-8-mediated apoptosis in T cells.

Introduction

The multitude of cell death mechanisms identified to date include the Fas/Fas ligand (FasL) system. Fas (1,2) is a member of the tumor necrosis factor (TNF) receptor family. After ligation and oligomerization by FasL, Fas recruits the Fas-associated death domain protein through interaction mediated by their respective death domains. Fas-associated death domain protein recruits caspase-8 and induces mitochondrial permeability transition (3) through voltage-dependent anion channel (VDAC) proteins. Bcl-2 family proteins, such as Bid and BAK, bind to VDAC proteins and regulate the mitochondrial membrane potential (4). Increased mitochondrial membrane permeability leads to the release of cytochrome C into the cytosol, which subsequently binds to dATP and Apaf-1, enabling engagement and activation of procaspase-9. Upon recruitment to the apoptosome, procaspase-3 is activated and, together with other downstream proteases, induces cell death that is termed apoptosis. VDAC proteins constitute the major pathway for metabolic exchange across the mitochondrial outer membrane. The existence of three mammalian isoforms (VDAC1, VDAC2 and VDAC3) suggests that they may each have some distinct physiological role. VDAC2 selectively prevents BAK activation and inhibits the mitochondrial apoptotic signal (5).

The Fas/FasL system is associated with the cytotoxic mechanism of immune cells. Some Fas-positive tumor cells are killed via the stimulation of Fas by FasL on activated T cells. The loss of Fas expression results in immune escape of tumor cells. In addition to tumor cells, activation-induced FasL expression and the engagement of Fas on activated T cells are responsible for activation-induced cell death of T cells themselves. T-cell activation was also shown to cause sensitization to Fas-mediated apoptosis (6–11).

Previously, we developed a monoclonal anti-Fas antibody, 2D1, which is capable of inducing apoptotic cell death. The Fas-sensitive T-leukemia lines Jurkat and SUP-T13 were cultured with the anti-Fas antibody, and stable Fas-resistant variant clones, Jurkat-FasR and SUP-T13-FasR were established after limiting dilution (12). These variant cells demonstrated phenotypes identical to those of the original cells, including cell surface Fas expression and antiapoptotic Bcl-2 protein expression. The Fas-resistant cells were as sensitive as the original cells to other apoptosis-inducing stimuli such as stimulation with γ-irradiation and calcium ionophore A23187.

To determine the molecular mechanism of Fas resistance of these variant cells, we performed comparative gene expression analysis using a DNA microarray to examine the differences in gene expression between Fas-sensitive clones and Fas-resistant clones. Among the genes that were overexpressed in Fas-resistant clones, esophageal cancer-related gene 4 (ECRG4) encoded a transmembrane protein that contained a porin/VDAC-like structure. ECRG4 was previously identified as one of the downregulated genes in esophageal cancer tissues (13). Therefore, we focused on the subcellular localization and function of ECRG4 in Fas-induced apoptosis. ECRG4 was detected in the mitochondria and endoplasmic reticulum. Overexpression of ECRG4 in Fas-sensitive Jurkat cells and RNA interference-mediated knockdown of ECRG4 in Fas-resistant Jurkat cells revealed a suppressive function of ECRG4 in Fas-induced apoptosis. Our study shows for the first time a novel function of ECRG4 in negative regulation of caspase-8-mediated apoptosis and suggests the involvement of this gene in the sensitivity of human T cells to activation-induced cell death.

Abbreviations: cDNA, complementary DNA; FasL, Fas ligand; MA, monoclonal antibody, mRNA; messenger RNA, PBS; phosphate-buffered saline, RT–PCR; reverse transcription–PCR, SDS; sodium dodecyl sulfate, siRNA; small interfering RNA, TNF; tumor necrosis factor, VDAC, voltage-dependent anion channel protein.

Materials and methods

Cell lines and culture conditions

Human embryonic kidney cell line 293T cells were cultured in Dulbecco's modified Eagle's medium (Sigma–Aldrich, St. Louis, MO) with 10% heat-inactivated fetal bovine serum and with 100 U/ml penicillin G and 100 μg/ml streptomycin. Jurkat and SUP T-13 cells were maintained in culture in RPMI 1640 (Sigma–Aldrich) supplemented with 10% fetal bovine serum, 100 U/ml penicillin G and 100 μg/ml streptomycin and were maintained at 37°C in a humidified 5% CO_2 atmosphere. The Fas-resistant Jurkat variant clone and Fas-resistant SUP T-13 variant clone were established and characterized previously (12). All of these cells were cultured at 37°C in a humidified 5% CO_2 atmosphere.

DNA microarray analysis

Total RNA was isolated from cultured cells by using an RNeasy Mini Kit (Qiagen, Valencia, CA) and treated with DNase I (Qiagen). Cy3- and Cy5-labeled amino-allyl amplified RNAs were prepared from the purified RNA by using an amino-allyl RNA amplification kit (Sigma-Genosys, Japan) according to the manufacturer's protocol. The labeled antisense RNAs were hybridized to high-density oligonucleotide arrays (Panorama Human Microarray; Sigma-Genosys) covering ~29 000 genes, and the fluorescence levels were analyzed using a Genepix 4000B (Axon Instruments).

Reverse transcription–PCR and quantitative PCR

A set of complementary DNAs (cDNAs) from normal human adult tissues (multiple tissue cDNA panels) was purchased from Clontech (Palo Alto, CA).

The cDNA mixture was synthesized by reverse transcription using SuperScript III and oligo(dT) primer (Invitrogen, Carlsbad, CA) according to the manufacturer's protocol. For detection of messenger RNA (mRNA) expression, reverse transcription–PCR (RT–PCR) was performed as follows. Briefly, PCR amplification was done in a 25 μl PCR mixture containing 1 μl of the cDNA, 1 μl of KOD Dash DNA polymerase (Toyobo, Osaka, Japan) and 200 pmol primers. The PCR mixture was initially incubated at 94°C for 5 min followed by 30 cycles of denaturation at 94°C for 30 s, annealing at 60°C for 2 s and extension at 74°C for 30 s. For specific detection of *ECRG4*, RT–PCR analysis was performed using the primer pair 5′-AAACGAGAAGCACCTGTTCC-3′ and 5′-GTAGTTGACGCTGGCTCCAT-3′ as forward and reverse primers, respectively. As an internal control, *GAPDH* was detected by using the forward primer 5′-CGAGATCCCTCCAAAATCAA-3′and reverse primer 5′-GTCTTCTGGGTGGCAGTGAT-3′. Real-time PCR was performed using an ABI-PRISM 7900 according to the protocol of the manufacturer (Applied Biosystems, Foster City, CA). Target gene expression was calculated using ΔΔCT and comparative methods after normalization to *GAPDH* expression.

Tissue samples

Tissue specimens were obtained from patients who underwent surgery at Kushiro City General Hospital. Tumor tissues and corresponding normal tissues were frozen at −80°C. Patients and their families gave informed consent for the use of tissue specimens in research.

Plasmids and transfection

To construct expression plasmids, total RNA was extracted from the Fas-resistant Jurkat clone, and cDNA was synthesized from the RNA by reverse transcription. Full-length *ECRG4* with an N-terminal myc epitope tag was amplified by using specific forward and reverse primers including NheI and XhoI restriction sites. The PCR product was purified and cloned into mammalian expression vector pcDNA3.1 (Invitrogen). Full-length *ECRG4* with a C-terminal flag epitope tag was amplified by using specific forward and reverse primers including BamHI and XhoI restriction sites and cloned into mammalian expression vector pcDNA3.1. Similarly, the PCR product of full-length *ECRG4* with a C-terminal flag epitope tag was produced and cloned into XhoI and BamHI restriction sites of the pIRES-EGFP2 vector (Clontech). The resulting pIRES-EGFP2-ECRG4 flag was digested with Nhe I and BamHI, and the cDNA fragment was cloned into vector pIRESpuro3 (Clontech). Similarly, full-length *ECRG4* was amplified by using specific forward and reverse primers including XhoI and HindIII restriction sites and cloned into pEGFP-N1 (Clontech). 293T cells and HeLa cells were transfected by using Lipofectamine 2000 reagent (Invitrogen). For stable transfection, Jurkat cells were transfected with plasmid pIRESpuro3-ECRG4 by using a Cell Line Nucleofector Kit V (Amaxa Biosystems). Two days after the transfection, transfected cells were selected in a medium containing 1.0 μg/ml puromycin.

Confocal laser microscopy

The method for confocal laser microscopy was described previously (14). After transfection with plasmid pEGFP-N1-ECRG4, which encoded ECRG4-EGFP fusion protein, HeLa cells were cultured on a glass coverslip (Fisher Scientific, Pittsburgh, PA), fixed in 4% paraformaldehyde and permeabilized in 0.1% Triton X-100. After blocking of cells with 3% bovine serum albumin for 1 h at room temperature, the cells were incubated with a monoclonal anti-KDEL antibody (Stressgen Bioreagents, Victoria, Canada), anti-golgin-97 antibody (Molecular Probes), mitotracker (Molecular Probes) or anti-β-actin antibody (Clone AC-15; Sigma) to detect the subcellular localization of ECRG4 protein. After washing with phosphate-buffered saline (PBS), cells were immunostained with rhodamine-conjugated anti-mouse IgG antibodies (KPL, Gaithersburg, MD), followed by visualization using a confocal laser microscope (Pascal; Carl Zeiss, Tokyo, Japan).

Cell proliferation assay

Cell proliferation was assessed by using an assay based on cleavage of tetrazolium salt WST-1 to formazan by cellular mitochondrial dehydrogenases. With this assay, a change in the number of viable cells results in a change in overall activity of the mitochondrial dehydrogenases in the sample. Augmentation of the enzyme activity leads to an increase in the amount of formazan dye formed. The formazan dye formed was quantified by using a plate reader. Briefly, cells were suspended at a concentration of 0.5–2 × 10^4 cells in 100 μl of culture medium per well on 96-well flat-bottom plates (Corning, NY) for 24–96 h. Apoptosis was induced by incubating cells with various concentrations of anti-Fas antibody CH11 (MBL, Japan), TNF alpha (Wako, Japan), Etoposide (Sigma) or staurosporine (Wako) for 24 h. Then a 1/10 volume of Premix WST-1 (Takara) was added to each well and the plates were incubated at 37°C for 2–4 h. The optical density of each well was quantified by using a microplate reader (Model 680 microplate reader, Bio-Rad). The test wavelength was 450 nm and the reference one was 655 nm.

Annexin-V labeling assay and detection of changes in mitochondrial membrane permeability

First, 1 × 10^6 Jurkat-pIRESpuro3-ECRG4 cells and Jurkat-pIRESpuro3 cells were plated on six-well tissue culture dishes with complete medium. Apoptosis was induced by incubating cells with various concentrations of anti-Fas antibody CH11 (MBL). Following the induction of apoptosis, apoptotic cells were labeled with an Annexin-V-FLUOS Staining kit (Roche Diagnostics). Briefly, the cell pellet was washed with PBS and resuspended in 100 μl of a staining solution containing Annexin-V-FLUOS and propidium iodide. After 15 min incubation at room temperature, cells were analyzed by using a fluorescence-activated cell sorter (FACS Calibur and Cell Quest software; BD Biosciences). For detection of changes in mitochondrial transmembrane potential, the MitoCapture™ Mitochondrial Apoptosis Detection Kit (MBL) was used. Briefly, 1.5–5 × 10^5 cells were pelleted following drug treatment and resuspended in 1 ml of prewarmed incubation buffer and 1 μl of MitoCapture. The cells were then incubated at 37°C in a humidified 5% CO_2 atmosphere for 15 min, pelleted, resuspended in 1 ml of incubation buffer and analyzed by flow cytometry.

Small interfering RNA-mediated knockdown of endogenous ECRG4

Synthetic ready to use small interfering RNA (siRNA) (21 nucleotides, stealth RNAi) and stealth RNAi negative control were purchased from Invitrogen. Small interfering RNA was introduced into Jurkat and Jurkat-FasR by using Nucleofector Device (Amaxa Inc.) and Cell Line Nucleofector Kit V (Amaxa) according to the manufacturer's protocol.

Western blotting

Cultured cells were washed in ice-cold PBS, homogenized in ice-cold radioimmunoprecipitation assay buffer (150 mmol/l NaCl, 1.0% NP40, 0.5% deoxycholic acid, 0.1% sodium dodecyl sulfate (SDS), 50 mmol/l Tris–HCl [pH 8.0], protease inhibitor cocktail [Complete; Roche Diagnostics, Basel, Switzerland]) for 30 min and clarified by centrifugation at 12 000*g* for 20 min at 4°C. The lysates were boiled for 5 min with SDS sample buffer and then separated by 12.5% or 15%

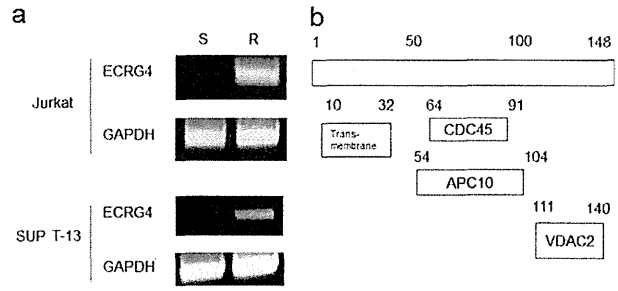

Fig. 1. Expression of *ECRG4* in Fas-resistant variants and the structure of ECRG4. (**a**) *ECRG4* mRNA expression was detected by RT–PCR in Fas-sensitive parental cells (S) and Fas-resistant variant (R) Jurkat cells (upper panel) and SUP-T13 cells (lower panel). *GAPDH* mRNA expression was detected in all of the cells. (**b**) ECRG4 has a transmembrane domain in the N-terminal region (amino acids 10–32), CDC45 homology domain (amino acids 64–91) and APC10 homology domain (amino acids 54–104) in the middle region, and VDAC2 homology domain (amino acids 111–140) in the C-terminal region of the protein. (**c**) Amino acid sequence of ECRG4. The predicted transmembrane region is indicated in italics, and the VDAC2 homology domain in the C-terminus is shown in underlined bold face in the amino acid sequence. (**d**) The amino acid sequence of the VDAC2 homology region in ECRG4 is aligned with the amino acid sequence of VDAC2. The VDAC homology domain of ECRG4 showed significant homology with VDAC2 (28% identity [9/32] and 50% similarity [16/32]). APC10, anaphase-promoting complex subunit 10; CDC45, cell division cycle 45; VDAC, voltage-dependent anion-selective channel.

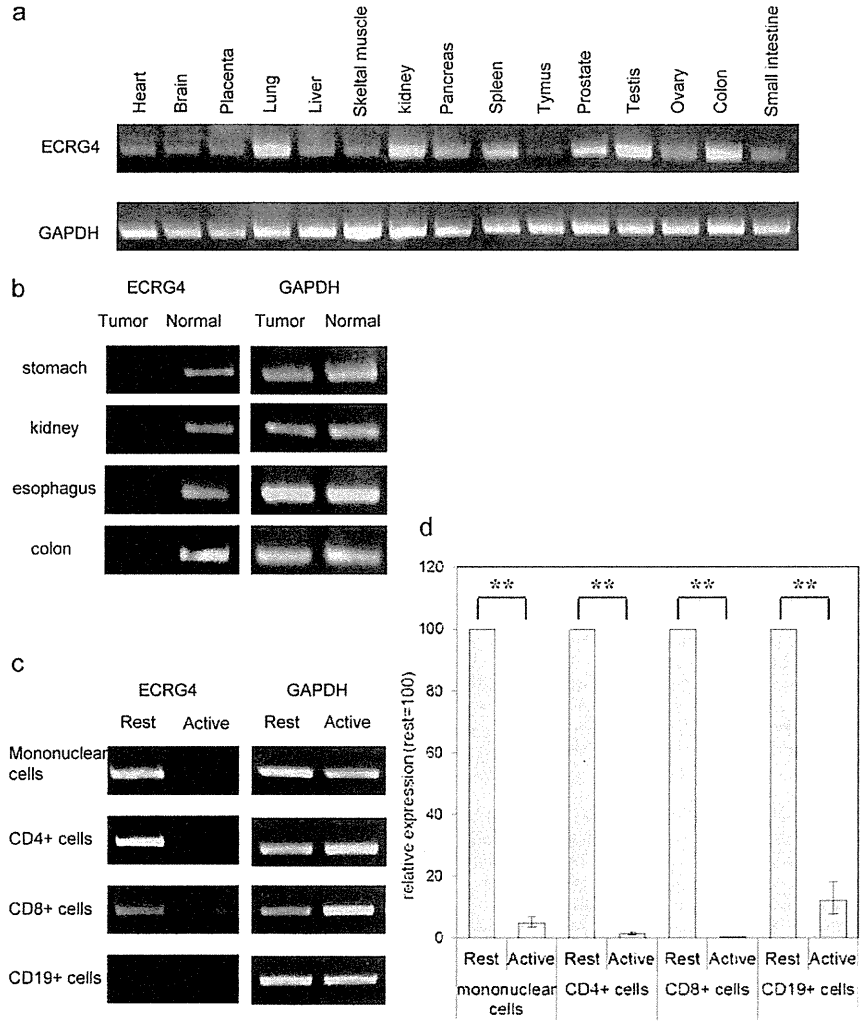

Fig. 2. Expression of *ECRG4* mRNA in normal human adult tissues, lymphocytes and tumor tissues. (**a**) cDNA samples from normal human adult tissues were analyzed for the expression of *ECRG4* and *GAPDH* by RT–PCR with specific primers. (**b**) Expression of *ECRG4* mRNA was determined by RT–PCR in tissue pairs of carcinoma tissues (tumor) and noncancerous tissues (normal) derived from surgical specimens of the same patients with gastric cancer, kidney cancer, esophageal cancer or colon cancer. (**c**) cDNA samples from peripheral blood mononuclear cells, resting and activated CD4+ T cells, resting and activated CD8+ T cells and resting and activated CD19+ T cells were analyzed for the expression of *ECRG4* and *GAPDH* by RT–PCR. For the activation of cells, mononuclear cells were activated with 2 μg/ml PWM (pokeweed mitogen, Gibco) and 5 μg/ml Con A (concanavalin A, ICN) for 3 days. CD4+ T cells were activated with 5 μg/ml Con A for 3–4 days. CD8+ T cells were activated with 5 μg/ml PHA (phytohemagglutinin, Pan Eco, Russia) for 3 days. CD19+ cells were activated with 2 μg/ml PWM. (**d**) *ECRG4* expression in activated lymphocyte cells compared with that in resting lymphocyte cells (resting cells = 100) was analyzed by real-time PCR. Data represent the averages of triplicate samples and the standard deviation. $^{**}P < 0.01$, unpaired *t*-test.

SDS–polyacrylamide gel electrophoresis. The proteins were transferred electrophoretically to polyvinylidene fluoride membranes (Immunobilon-P; Millipore, Billerica, MA). The membranes were incubated with blocking buffer (5% nonfat dry milk in PBS) at room temperature and then incubated for 60 min with the following monoclonal antibodies (mAbs): mouse anti-Flag mAb m2 (Sigma–Aldrich), mouse anti-myc mAb 9E10, mouse anti-caspase-8 mAb 12F5 (Invitrogen), rabbit anti-Bid Ab (Abcam, UK) and mouse anti-β-actin mAb AC-15 (Sigma–Aldrich). After washing three times with wash buffer (0.1% Tween 20, PBS), the membranes were reacted with a peroxidase-labeled secondary antibody (peroxidase-labeled goat anti-mouse IgG or anti-rabbit IgG; KPL) for 30 min. Finally, the signal was visualized by using an enhanced chemiluminescence detection system (Amersham Life Science, Arlington Heights, IL) according to the manufacturer's protocol.

Caspase activity assay

First, 3 × 10^6 Jurkat-pIRESpuro3-ECRG4 cells and Jurkat-pIRESpuro3 cells were plated on six-well tissue culture dishes with complete medium. Apoptosis was induced by incubating cells with 100 ng/ml of anti-Fas antibody CH11 (MBL). The activities of caspase-8 or -3 were measured by using a APOPCYTO Caspase-8 or -3 Colorimetric Assay Kit (MDL) according to the manufacturer's protocol. Briefly, 3 × 10^6 cells were collected, resuspended in ice-cold cell lysis buffer and incubated on ice for 10 min. Then 50 μl of reaction buffer containing 10 mM dithiothreitol was added to each well of a 96-well microplate, followed by incubation at 37°C for 4 h with 5 μl of caspase-8 substrate IETD-*p*NA or caspase-3 substrate DEVD-*p*NA. The absorbance at 405 nm was measured by using a microplate reader.

Immunoprecipitation assay

293T cells were washed, pelleted and resuspended in a lysis buffer supplemented with protease inhibitors (10 mM *N*-2-hydroxyethylpiperazine-*N*′-2-ethanesulfonic acid, pH 8.0, 150 mM NaCl, 1% 3-[(3-Cholamidopropyl)dimethylammonio]-propanesulfonate, protease inhibitor cocktail). The cell lysate was precleaned, and the supernatant was incubated for 3 h with anti-FLAG or anti-procaspase-8 (Upstate, NY) on a rotation platform at 4°C, followed by incubation with protein G-sepharose beads (GE Healthcare). Beads were collected, washed and resuspended in an equal volume of SDS sample buffer. The beads were boiled for

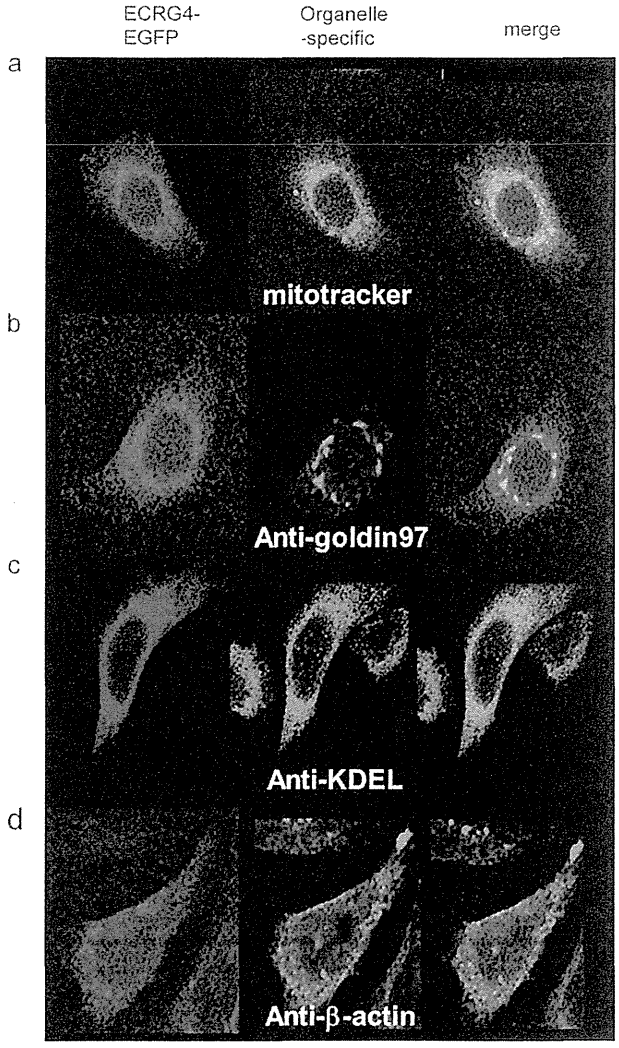

Fig. 3. Determination of subcellular localization of ECRG4-EGFP in HeLa cells. An expression plasmid encoding ECRG4-EGFP fusion protein was introduced into HeLa cells, and the fusion protein was detected as green fluorescence by confocal laser microscopy. Subcellular organelles were visualized by red fluorescence staining with a fluorescent probe or antibodies against organelle-specific markers including the mitochondrial marker MitoTracker Red 580 (**a**), Golgi apparatus marker anti-golgin-97 (**b**), endoplasmic reticulum marker anti-KDEL (**c**) and cytoskeletal marker anti-β-actin (**d**).

5 min with SDS sample buffer and then separated by 12.5% or 15% SDS-polyacrylamide gel electrophoresis. The western blot assay was performed as described above using appropriate antibodies

Statistical analysis

Statistical differences between groups were evaluated using a two-tailed Student's *t*-test or one-way analysis of variance as appropriate, with P values <0.05 considered significant.

Results

Comparative gene expression analysis of Fas-sensitive cells and Fas-resistant variants

To elucidate the differences in gene expression between Fas-sensitive Jurkat cells and Fas-resistant variant Jurkat FasR cells, we used a cDNA microarray and performed comparative gene expression analysis. Amplified antisense RNA was labeled with Cy3 or Cy5 and hybridized to an oligonucleotide DNA microarray covering ~29 000 human genes. A dye swapping experiment was performed for the same RNA samples to exclude artifact changes. cDNA microarray data are summarized in Supplementary Table 1 available at *Carcinogenesis* Online. As a result of the analysis, several genes that might be aberrantly expressed in Jurlat-FasR cells were found. We then screened the genes by semi-quantitative RT–PCR to confirm the increased expression in Fas-resistant variants. Of the screened genes, esophageal cancer-related gene 4 (*ECRG4*) was noted since it showed a 64-fold higher expression level in Jurkat FasR cells than in Fas-sensitive parental Jurkat cells. *ECRG4* was also expressed aberrantly in Fas-resistant SUP T-13 variant SUP T-13-FasR cells (Figure 1a).

Expression of ECRG4 mRNA in normal tissues, tumor tissues and lymphocytes

To elucidate the distribution of *ECRG4*, we investigated the expression profile of *ECRG4* in normal human adult tissues. *ECRG4* mRNA expression was detected ubiquitously in normal adult tissues (Figure 2a). Since a previous report showed that ECRG4 was downregulated in cancerous tissues in the esophagus compared with its expression level counterpart normal esophageal mucosa, the expression of *ECRG4* mRNA was determined in several pairs of tumor tissues and corresponding normal tissues derived from surgical specimens of the same patient (one esophageal cancer, four stomach cancers, four colon cancers, two liver cancers and two kidney cancers). *ECRG4* mRNA expression was downregulated in 11 of the 13 tumor tissues (Figure 2b). The data were basically compatible with a previous report (13).

Since *ECRG4* was upregulated in Fas-resistant Jurkat cells, we investigated the expression of *ECRG4* in immunocytes in both resting and activated states. RT-PCR and real-time PCR showed that *ECRG4* was expressed in peripheral blood mononuclear cells, CD4-positive T cells, CD8-positive T cells and CD19-positive B cells in a resting state; however, *ECRG4* was downregulated in those cells in an activated state (Figure 2c and d).

Domain structure of ECRG4 protein

ECRG4 was previously identified as one of the downregulated genes in esophageal cancer cells (13). However, the function of ECRG4 has not been elucidated yet. To examine the function of ECRG4, we performed a homology domain search by using a public protein structure database. Analysis using the SMART database (http://smart.embl-heidelberg.de/) revealed that ECRG4 had one transmembrane segment starting at amino acid position 10 and ending at amino acid position 32 (Figure 1c, italics). By analysis using the BLOCKS database (http://bioinfo.weizmann.ac.il/blocks/blocks_search.html), it was further revealed that ECRG4 contained a porin/VDAC homology domain (amino acids 111–140), a cell division cycle 45 (Cdc45) homology domain (amino acids 64–91) and an anaphase-promoting complex subunit 10 (APC 10) homology domain (amino acids 54–104) (Figure 1b). The amino acid sequence of the VDAC homology domain of ECRG4 (Figure 1c, underlined bold face) is aligned with that of VDAC2 in Figure 1d. The amino acid sequence of the VDAC homology domain of ECRG4 showed significant homology with that of VDAC2 (28% identity [9/32 amino acids] and 50% similarity [16/32 amino acids]) (Figure 1d). The structural characterization indicated that ECRG4 might be a transmembrane protein that is associated with mitochondrial membrane permeability and cell cycle.

Subcellular localization of ECRG4

To determine the subcellular localization of ECRG4, an expression plasmid encoding ECRG4-EGFP fusion protein was introduced into HeLa cells, and the fusion protein was detected by confocal laser microscopy. Subcellular organelles were visualized by immunofluorescence staining with antibodies against organelle-specific markers such as the mitochondria marker MitoTracker Red 580, Golgi apparatus marker golgin-97, endoplasmic reticulum marker amino acid

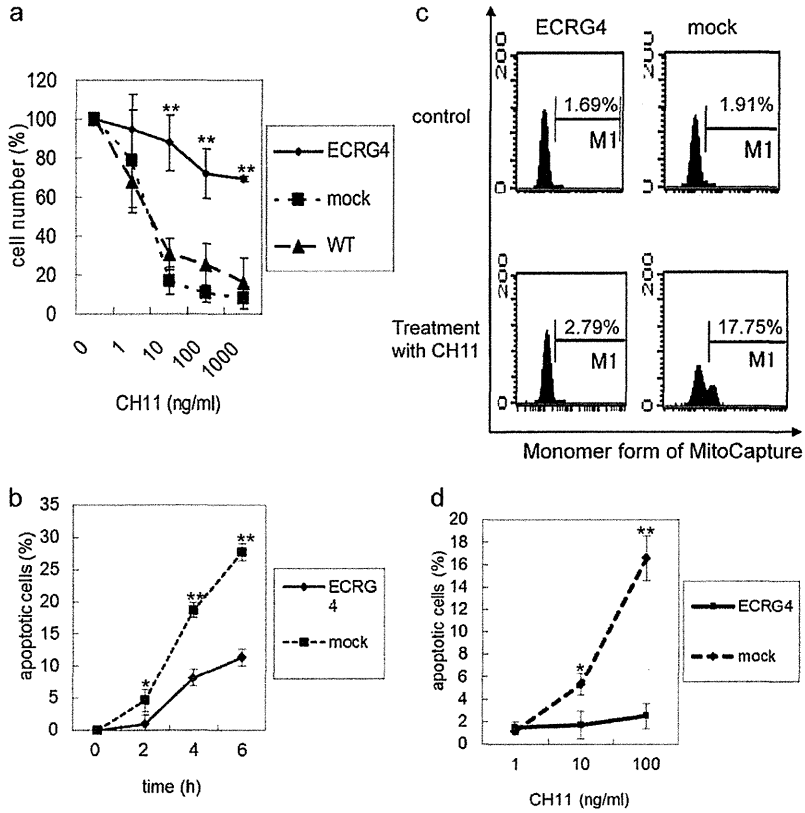

Fig. 4. Sensitivity of ECRG4-expressing Jurkat cells to Fas-induced apoptosis. (**a**) Jurkat transfectants (1×10^3) were plated on 96-well tissue culture dishes. Apoptosis was induced by incubating cells with the indicated concentrations of anti-Fas antibody CH11. After 24 h, viable cell numbers were analyzed by WST-1 assay. Data represent the averages of triplicate samples and the standard deviation. $^{**}P < 0.01$, analysis of variance. (**b**) Jurkat transfectants (7×10^5) were plated on a six-well tissue culture dish. Apoptosis was induced by incubating cells with 100 ng/ml anti-Fas antibody CH11 for the indicated time. Cells were stained with annexin-V-FLUOS and propidium iodide and then analyzed by flow cytometry. Data represent the averages of triplicate samples and the standard deviation. $^{*}P < 0.05$; $^{**}P < 0.01$, unpaired *t*-test. (**c**) Mitochondrial membrane permeability transition was assessed using a MitoCapture fluorescent probe. Jurkat transfectants (1.5×10^5) were plated on a six-well tissue culture dish. Apoptosis was induced by incubating cells with 100 ng/ml anti-Fas antibody CH11 for 120 min. The monomer form of MitoCapture was detected as green fluorescence by flow cytometry, representing mitochondrial transmembrane potential change. (**d**) Apoptosis was induced by incubating cells with the indicated concentrations of anti-Fas antibody CH11. Apoptotic cell rates were assessed on the basis of the percentage of the monomer form of MitoCapture by flow cytometry. Data represent the averages of triplicate samples and the standard deviation. $^{*}P < 0.05$; $^{**}P < 0.01$, unpaired *t*-test.

sequence KDEL and cytoskeletal marker β-actin. The confocal laser microscopy showed that ECRG4 was colocalized with MitoTracker Red 580, anti-golgin-97 Ab and anti-KDEL Ab but not with anti-β-actin Ab in HeLa cells (Figure 3a–d). These findings indicated that ECRG4 was localized in the mitochondria, Golgi apparatus and endoplasmic reticulum.

ECRG4-expressing Jurkat cells acquired resistance to Fas-induced apoptosis

ECRG4 was upregulated in apoptosis-resistant Jurkat FasR cells and SUP T-13-FasR cells, and it was expressed in resting immunocytes, which are resistant to apoptosis. And part of ECRG4 protein is localized to mitochondria which has role in induction of apoptosis. Therefore, we further investigated ECRG4 roles in apoptosis. To determine whether the increased ECRG4 levels conferred resistance to Fas-induced apoptosis in Jurkat cells, we established stable ECRG4-expressing cells by gene transfection. The obtained Jurkat ECRG4 cells were characterized by RT–PCR (Supplementary Figure 1A, available at *Carcinogenesis* Online) and western blotting (Supplementary Figure 1B, available at *Carcinogenesis* Online). By flow cytometric analysis, it was confirmed that Jurkat ECRG4 cells had a level of Fas expression on the cell surface that was almost identical to that on the control Jurkat mock cells (Supplementary Figure 1C, available at *Carcinogenesis* Online).

Next, the sensitivity to Fas stimulation was compared among parental Jurkat cells, Jurkat mock cells and Jurkat ECRG4 cells. The cell viability was assessed by WST-1 assay and apoptotic cell death rate was assessed by annexin-V/propidium iodide-labeling assay, respectively. In the WST-1 assay, Jurkat ECRG4 cells showed a significantly higher survival rate at various concentrations of the anti-Fas antibody than the survival rates of parental Jurkat cells (Jurkat-WT) and Jurkat mock cells (Figure 4a). In the annexin-V/propidium iodide-labeling assay, the percent of cells showing annexin-V was less for Jurkat ECRG4 cells than for Jurkat mock cells (Figure 4b). These observations indicate that Jurkat ECRG4 cells are resistant to apoptosis by Fas stimuli.

Expression of ECRG4 inhibits mitochondrial membrane permeability transition

Since ECRG4 was estimated to contain a VDAC homology domain and it was localized on mitochondria, we investigated whether ECRG4 expression could affect mitochondrial membrane depolarization and permeability. MitoCapture, a cationic dye, provides a fluorescence-based molecular probe for detecting changes in mitochondrial

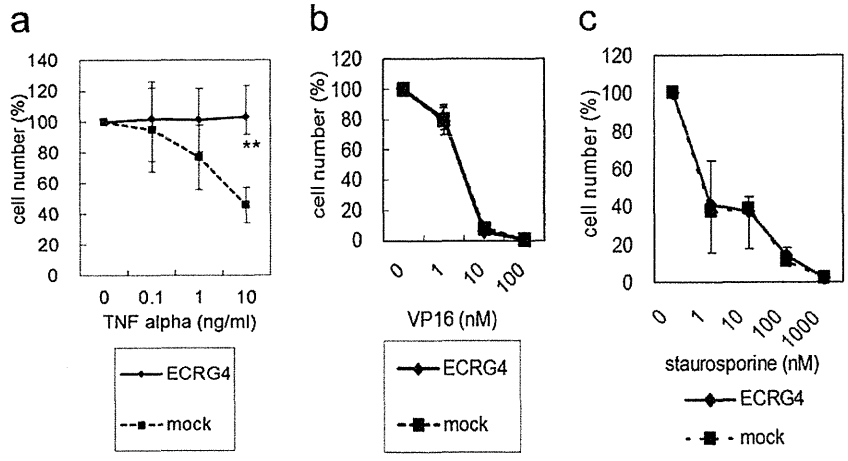

Fig. 5. Overexpression of ECRG4 suppresses TNF-alpha-mediated apoptosis. Jurkat transfectants (1×10^4) were plated on 96-well tissue culture dishes. Apoptosis was induced by incubating cells with the indicated concentrations of TNF-alpha (**a**), etoposide (**b**) and staurosporine (**c**). After 24 h, viable cells were analyzed by WST-1 assay. Data represent the averages of triplicate samples and the standard deviation. $^{**}P < 0.01$, unpaired *t*-test.

transmembrane potential. In healthy cells, MitoCapture accumulates and aggregates in the mitochondria, giving off red fluorescence. In apoptotic cells, MitoCapture remains in the cytoplasm in its monomer form due to the altered mitochondrial transmembrane potential, thus giving off green fluorescence.

In control Jurkat mock cells, green fluorescence-positive cells derived from the monomer form of MitoCapture were increased after stimulation with anti-Fas antibody CH11; however, in Jurkat ECRG4 cells, green fluorescence-positive cells were not increased after the same stimulation (Figure 4c). Fas stimulation induced a concentration-dependent increase in the monomer form of MitoCapture in control cells, whereas it failed to induce the monomer form in ECRG4-expressing Jurkat cells (Figure 4d). The activities of caspase-3 were significantly suppressed in ECRG4-expressing Jurkat cells (Supplementary Figure 2A, available at *Carcinogenesis* Online). These findings indicated that ECRG4 expression inhibited apoptosis through suppressing mitochondrial membrane depolarization and permeability.

Knockdown of endogenous ECRG4 increases sensitivity to Fas-mediated apoptosis

To confirm the antiapoptotic function of ECRG4, we investigated whether decreases in endogenous ECRG4 levels alter the sensitivity to Fas-mediated apoptosis. Since an anti-ECRG4 antibody was not available for detection of endogenous ECRG4 protein, we assessed the efficacy of RNA interference by RT–PCR. We tested three different siRNA duplexes designed to target ECRG4 and confirmed that ECRG4-specific siRNA2 was the most effective in decreasing endogenous ECRG4 mRNA level in Jurkat FasR cells (Supplementary Figure 3A, available at *Carcinogenesis* Online). After culture of siRNA transfected cells in media containing various concentrations of anti-Fas antibodies for 48 h, live cell rates were assessed by the WST-1 assay. It was shown that knockdown of endogenous ECRG4 mRNA leads to decreases in survival rate after Fas stimulation of Jurkat FasR cells (Supplementary Figure 3B, available at *Carcinogenesis* Online). After culture of siRNA transfected cells in a medium containing 100 ng/ml anti-Fas antibody for 1 h, early apoptotic cells with increased mitochondrial membrane permeability were assessed by the MitoCapture assay. It was shown that knockdown of endogenous ECRG4 increases the sensitivity to Fas-mediated alterations of mitochondrial membrane depolarization in Jurkat FasR cells (Supplementary Figure 3C, available at *Carcinogenesis* Online), suggesting that ECRG4 is involved in the negative regulation of Fas-induced apoptotic signals, at least in part, at the level of mitochondria or the upstream level of mitochondria in Jurkat cells.

Overexpression of ECRG4 suppresses TNF-alpha-induced apoptosis in Jurkat cells

ECRG4 has a suppressive role in apoptosis induced by Fas probably by inhibiting mitochondrial membrane depolarization and permeability, we extended our focus to other apoptosis stimuli including TNF-alpha, etoposide and staurosporine. Sensitivity to apoptotic stimuli was assessed by the WST-1 assay. Jurkat ECRG4 cells showed a significantly higher survival rate at various concentrations of TNF-alpha than that of Jurkat mock cells (Figure 5a). Etoposide, a well-known cancer chemotherapeutic agent, is an inhibitor of topoisomerase II and induces p53-dependent apoptosis (15). Jurkat-ECRG4 and control cells showed almost identical sensitivities to etoposide-induced apoptosis (Figure 5b). Staurosporine is a protein kinase inhibitor and induces apoptosis independently of caspase-8 activation (16). Jurkat ECRG4 and control cells showed almost identical sensitivities to staurosporine-induced apoptosis (Figure 5c). These results indicated that ECRG4 suppresses caspase-8-dependent apoptosis but does not suppress caspase-8-independent apoptosis.

Overexpression of ECRG4 suppresses the activity of caspase-8

To elucidate the exact molecular mechanism by which ECRG4 suppresses caspase-8-mediated apoptosis, the following experiments were performed. Bid is known as a proapoptotic molecule (17) that functions upstream of mitochondria in caspase-8-dependent apoptotic signals (18). To determine the intracellular signaling events in ECRG4-expressing cells, we examined cleavage of caspase-8 and Bid in Jurkat ECRG4 cells after stimulation with anti-Fas mAb. As shown in Figure 6a, cleaved caspase-8 subunit p18 was detected at similar levels in ECRG4 transfectants and mock control cells; however, truncated Bid was not detected in ECRG4-expressing Jurkat cells. Next, we examined activities of caspase-8 in Jurkat transfectant cells after stimulation with anti-Fas mAb. The activities of caspase-8 were significantly suppressed in ECRG4-expressing Jurkat cells (Figure 6b). Immunoprecipitation results demonstrated that ECRG4 was associated with procaspase-8 (Figure 6c) but not with Bid (data not shown). The results clearly show that ECRG4 can be associated with procaspase-8 and suppress the activity of caspase-8, thus leading to the suppression of Fas-induced apoptosis.

Discussion

We identified and characterized a novel antiapoptotic molecule, ECRG4, which was aberrantly expressed in Fas-resistant T-cell variant clones. The ECRG4 gene was previously cloned from human normal

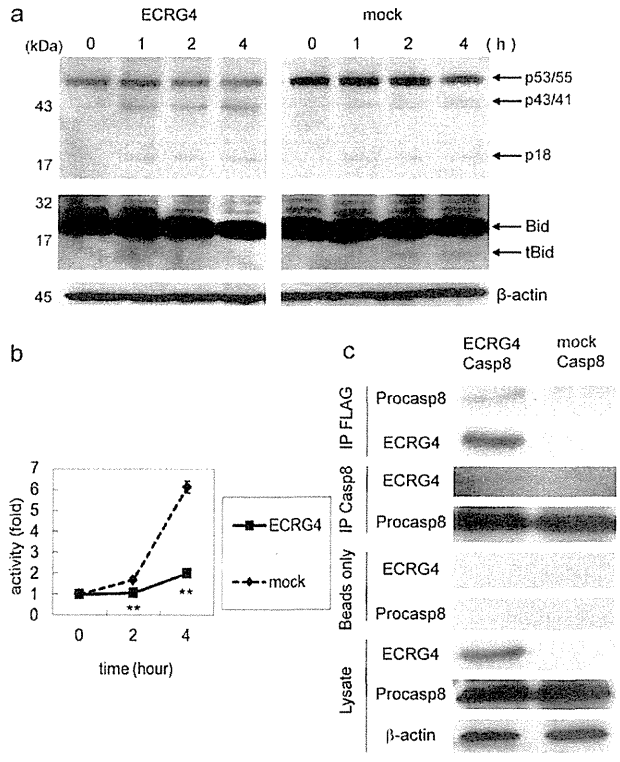

Fig. 6. Overexpression of ECRG4 suppresses caspase-8 activation and ECRG4 is associated with procaspase-8. (**a**) Jurkat transfectants (2×10^6) were plated on a 6 cm tissue culture dish. Apoptosis was induced by incubating cells with 100 ng/ml anti-Fas antibody CH11 for the indicated time. Procaspase-8, caspase-8, Bid, cleaved Bid and β-actin were detected by western blotting. (**b**) Jurkat transfectants (3×10^6) were plated on a culture dish. Apoptosis was induced by incubating cells with 100 ng/ml anti-Fas antibody CH11 for the indicated time. Following induction of apoptosis, the activities of caspase-8 were measured by using a APOPCYTO Caspase-8 Colorimetric Assay Kit. Data represent the averages of triplicate samples and the standard deviation compared with control cell activities. $^{**}P < 0.01$, unpaired *t*-test. (**c**) 293T cells were transfected with FLAG-tagged ECRG4 and procaspase-8, mock and procaspase-8 (control). Co-immunoprecipitation assay was performed using anti-FLAG, anti-procaspase-8 and without antibody (beads only). Immunoprecipitation assay demonstrated that ECRG4 is associated with procaspase-8.

esophageal epithelium and identified as one of the downregulated genes in esophageal squamous cell carcinoma tissues (13). The mechanism of gene inactivation in tumor tissues involves DNA methylation, and it is a frequent molecular event in esophageal squamous cell carcinoma (13). It was reported that low-*ECRG4* mRNA expression levels were associated with significantly short survival after surgery compared with high-*ECRG4* mRNA expression levels in esophageal cancer patients (19). Therefore, it has been speculated that ECRG4 is a tumor suppressor gene that is frequently inactivated in esophageal cancer cells. ECRG4 is also known as a senescence inducer (20). Cell senescence is defined as irreversible growth arrest. It acts as a potent barrier to tumorgenesis *in vivo*. In senescent cells, there is increased sensitivity with advance of age to the intrinsic pathway that regulates apoptosis. This sensitivity includes increased cell death in response to ultraviolet light, radiation, stress and other toxins. In contrast, there is generally an age-related decrease in apoptosis mediated through the extrinsic pathway. The extrinsic pathway is signaled through TNF receptor superfamily members, including Fas. A key regulator of apoptosis signals that operates within the intrinsic pathway is p53, whereas a key regulator of apoptosis signals that operates within the extrinsic pathway is caspase-8 (21). However, little is known about the function of ECRG4 in apoptosis.

In the present study, we examined the expression and function of ECRG4. Caspases are cysteine proteases that play a central role in apoptotic signals. Caspase-8 is the most upstream caspase in the proteolytic cascade that is activated by Fas ligand and TNF-alpha. During Fas-mediated apoptosis, procaspase-8 is recruited to the death-inducing signaling complex. Procaspase-8 is first cleaved into intermediate cleavage products and is subsequently processed to p18 subunits and p10 subunits. The heterodimer of p18 and p10 subunits is the active form of caspase-8. The active form of caspase-8 cleaves Bid, and the C-terminal part translocates to mitochondria, where it triggers cytochrome C release. While full-length BID is localized in the cytosol, truncated Bid translocates to mitochondria and thus transduces apoptotic signals from the cytoplasmic membrane to mitochondria.

FLICE inhibitory protein interacts with caspase-8 through distinct domains and suppresses Fas-induced apoptosis (22). Our data showed that ECRG4 also associated with procaspase-8 and suppressed the activation of caspase-8, leading to inhibition of the cleavage of Bid. Procaspase-8 is a precursor of caspase-8 and is also the full length of caspase-8. ECRG4 is associated with procaspase-8, which is the full length of caspase-8; however, the ECRG4-binding site in the full length of caspase-8 remains unclear. Since ECRG4 did not affect the cleavage of p18 subunits of caspase-8, it might inhibit the configuration of the active conformation of caspase-8.

ECRG4 contains a VDAC2-like domain that might be associated with apoptotic signals. Procaspase-8 localizes in both the mitochondria and the cytosol; however, active caspase-8 is localized in mitochondria by apoptotic stimulations (23). A native complex containing caspase-8 and Bid localized on the mitochondrial membrane and death receptor activation by Fas induced the cleavage of Bid within this complex. tBid then shifted to separate mitochondrial-associated complexes that contained other Bcl-2 family members, such as BAK and Bcl-xL (24). Our data showed that ECRG4 was also localized in mitochondria, suggesting that ECRG4 inhibits caspase-8 activation on the mitochondrial membrane, suppresses cleavage of Bid and leads to inhibition of the mitochondrial apoptosis pathway. VDAC2 is associated with BAK, leading to prevention of BAK activation and inhibition of the apoptosis pathway (5). Therefore, ECRG4 inhibited apoptosis at the upstream level of VDAC2 in the mitochondrial apoptosis signaling.

Our data revealed that ECRG4 is involved in the suppression of Bid cleavage and subsequent mitochondrial membrane permeability transition induced by Fas stimulation. Thus, ECRG4 may have an antiapoptotic function similar to that of VDAC2 on the mitochondrial outer membrane. It was noted that ECRG4 was localized not only to mitochondria but also to the endoplasmic reticulum and Golgi apparatus. Since it has been proposed that VDAC1 and the Bcl-2-family also reside and function in extramitochondrial membranes including the endoplasmic reticulum (25), ECRG4 may be involved in various cellular functions in multicompartment localization in concert with VDAC1 and the Bcl-2 family.

Our results and results of other studies show that ECRG4 expression is decreased in tumor tissues. Therefore, the antiapoptotic function of ECRG4 cannot explain the significance of ECRG4 in tumorigenesis. In this context, ECRG4 contains a CDC45- and APC10 homology domain, and ECRG4 expression inhibits the growth of various tumor cells (data not shown). It is possible that ECRG4 has both an antiapoptotic function and an antiproliferative function as reported for Bcl-2 family proteins (14,26–28). Besides the role of ECRG4 in tumorigenesis, it should be noted that ECRG4 might be involved in the development and fate of normal T cells. ECRG4 is expressed in peripheral resting T cells, but it is downregulated after their activation. The expression of ECRG4 may be associated with survival potential of naive T cells, and its downregulation after activation may be associated with activation-induced cell death mediated by Fas/FasL stimulation in both mature and immature T cells.

In conclusion, we have identified and characterized an antiapoptotic function of ECRG4. ECRG4 was found to be localized in the mitochondria, endoplasmic reticulum and Golgi apparatus. ECRG4 has a function of suppressing Fas-induced apoptosis through inhibition of

caspase-8 activity. Our results suggest that ECRG4 is a novel regulator of caspase-8-dependent apoptotic signals in human T cells.

Supplementary material

Supplementary Table 1 and Figures 1–3 can be found at http://carcin.oxfordjournals.org/.

Funding

Ministry of Education, Culture, Sports, Science and Technology of Japan (23590427), (21590401).

Conflict of Interest Statement: None declared.

References

1. Itoh,N. *et al.* (1991) The polypeptide encoded by the cDNA for human cell surface antigen Fas can mediate apoptosis. *Cell*, **66**, 233–243.
2. Oehm,A. *et al.* (1992) Purification and molecular cloning of the APO-1 cell surface antigen, a member of the tumor necrosis factor/nerve growth factor receptor superfamily. Sequence identity with the Fas antigen. *J. Biol. Chem.*, **267**, 10709–10715.
3. Chinnaiyan,A.M. *et al.* (1995) FADD, a novel death domain-containing protein, interacts with the death domain of Fas and initiates apoptosis. *Cell*, **81**, 505–512.
4. Shimizu,S. *et al.* (1999) Bcl-2 family proteins regulate the release of apoptogenic cytochrome c by the mitochondrial channel VDAC. *Nature*, **399**, 483–487.
5. Cheng,E.H. *et al.* (2003) VDAC2 inhibits BAK activation and mitochondrial apoptosis. *Science*, **301**, 513–517.
6. Green,D.R. *et al.* (2003) Activation-induced cell death in T cells. *Immunol. Rev.*, **193**, 70–81.
7. Brunner,T. *et al.* (1995) Cell-autonomous Fas (CD95)/Fas-ligand interaction mediates activation-induced apoptosis in T-cell hybridomas. *Nature*, **373**, 441–444.
8. Daniel,P.T. *et al.* (1994) Activation induces sensitivity toward APO-1 (CD95)-mediated apoptosis in human B cells. *J. Immunol.*, **152**, 5624–5632.
9. Dhein,J. *et al.* (1995) Autocrine T-cell suicide mediated by APO-1/(Fas/CD95). *Nature*, **373**, 438–441.
10. Ju,S.T. *et al.* (1995) Fas(CD95)/FasL interactions required for programmed cell death after T-cell activation. *Nature*, **373**, 444–448.
11. Mogil,R.J. *et al.* (1995) Fas (CD95) participates in peripheral T cell deletion and associated apoptosis *in vivo*. *Int. Immunol.*, **7**, 1451–1458.
12. Takahashi,S. *et al.* (1993) Establishment of apoptosis-inducing monoclonal antibody 2D1 and 2D1-resistant variants of human T cell lines. *Eur. J. Immunol.*, **23**, 1935–1941.
13. Yue,C.M. *et al.* (2003) Expression of ECRG4, a novel esophageal cancer-related gene, downregulated by CpG island hypermethylation in human esophageal squamous cell carcinoma. *World J. Gastroenterol.*, **9**, 1174–1178.
14. Schmitt,E. *et al.* (2007) Nuclear colocalization and interaction between bcl-xL and cdk1(cdc2) during G2/M cell-cycle checkpoint. *Oncogene*, **26**, 5851–5865.
15. Mahyar-Roemer,M. *et al.* (2001) p21 Waf1/Cip1 can protect human colon carcinoma cells against p.53-dependent and p.53-independent apoptosis induced by natural chemopreventive and therapeutic agents. *Oncogene*, **20**, 3387–3398.
16. Han,Z. *et al.* (1996) DNA-dependent protein kinase is a target for a CPP32-like apoptotic protease. *J. Biol. Chem.*, **271**, 25035–25040.
17. Wang,K. *et al.* (1996) BID: a novel BH3 domain-only death agonist. *Genes Dev.*, **10**, 2859–2869.
18. Luo,X. *et al.* (1998) Bid, a Bcl2 interacting protein, mediates cytochrome c release from mitochondria in response to activation of cell surface death receptors. *Cell*, **94**, 481–490.
19. Mori,Y. *et al.* (2007) Expression of ECRG4 is an independent prognostic factor for poor survival in patients with esophageal squamous cell carcinoma. *Oncol. Rep.*, **18**, 981–985.
20. Kujuro,Y. *et al.* (2010) Esophageal cancer-related gene 4 is a secreted inducer of cell senescence expressed by aged CNS precursor cells. *Proc. Natl Acad. Sci. USA*, **107**, 8259–8264.
21. Hsu,H.C. *et al.* (2005) Impaired apoptosis and immune senescence—cause or effect? *Immunol. Rev.*, **205**, 130–146.
22. Shu,H.B. *et al.* (1997) Casper is a FADD- and caspase-related inducer of apoptosis. *Immunity*, **6**, 751–763.
23. Chandra,D. *et al.* (2004) Association of active caspase 8 with the mitochondrial membrane during apoptosis: potential roles in cleaving BAP31 and caspase 3 and mediating mitochondrion-endoplasmic reticulum cross talk in etoposide-induced cell death. *Mol. Cell. Biol.*, **24**, 6592–6607.
24. Schug,Z.T. *et al.* (2011) BID is cleaved by caspase-8 within a native complex on the mitochondrial membrane. *Cell Death Differ.*, **18**, 538–548.
25. Shoshan-Barmatz,V. *et al.* (1996) VDAC/porin is present in sarcoplasmic reticulum from skeletal muscle. *FEBS Lett.*, **386**, 205–210.
26. Vairo,G. *et al.* (1996) Bcl-2 has a cell cycle inhibitory function separable from its enhancement of cell survival. *Oncogene*, **13**, 1511–1519.
27. Fujise,K. *et al.* (2000) Regulation of apoptosis and cell cycle progression by MCL1. Differential role of proliferating cell nuclear antigen. *J. Biol. Chem.*, **275**, 39458–39465.
28. Zinkel,S.S. *et al.* (2005) A role for proapoptotic BID in the DNA-damage response. *Cell*, **122**, 579–591.

Received October 25, 2011; revised February 10, 2012; accepted March 3, 2012

Pathology International

Pathology International 2012; **62**: 684–689 doi:10.1111/j.1440-1827.2012.02851.x

Original Article

High expression of ALDH1 and SOX2 diffuse staining pattern of oral squamous cell carcinomas correlates to lymph node metastasis

Yoshitaka Michifuri,[1,2] Yoshihiko Hirohashi,[1] Toshihiko Torigoe,[1] Akihiro Miyazaki,[2] Junichi Kobayashi,[2] Takanori Sasaki,[2] Jyunki Fujino,[2] Hiroko Asanuma,[3] Yasuaki Tamura,[1] Kenji Nakamori,[2] Tadashi Hasegawa,[3] Hiroyoshi Hiratsuka[2] and Noriyuki Sato[1]

Departments of [1]Pathology, [2]Oral Surgery, [3]Surgical Pathology, Sapporo Medical University School of Medicine, Sapporo, Japan

One of the major factors involved in the prognosis of oral squamous cell carcinoma (OSCC) patients is metastasis. Recent progress in cancer stem-like cell/cancer-initiating cell (CSC/CIC) research indicates that CSCs are related to metastasis. Aldehyde dehydrogenase 1 – (ALDH1) and SRY-related HMG-box gene 2 (SOX2) have recently been shown to be putative CSC markers for several human malignancies. The aim of this study was to determine the association of ALDH1 and SOX2 expression in oral squamous cell carcinoma (OSCC) with lymph node metastasis. Immunohistochemical staining of ALDH1, SOX2 and Ki67 was performed in 80 OSCC tissues. High expression rates of ALDH1 (2%–40%) were found to be related to lymph node metastasis ($P = 0.0017$). Interestingly, we found that SOX2 staining could be classified into two patterns: (i) peripheral staining pattern; and (ii) diffuse staining pattern. The diffuse staining pattern showed a significant correlation with lymph node metastasis ($P < 0.001$). No correlation was found between Ki67 staining and lymph node metastasis ($P = 0.4724$). The ALDH1 positive staining rates in metastatic lymph nodes were higher than that in corresponding primary OSCC tissues. These results indicate that high expression rates of ALDH1 and SOX2 diffuse staining patterns might be novel prediction markers for OSCC lymph node metastasis.

Key words: ALDH1, cancer stem cell, lymph node metastasis, oral squamous cell carcinoma, SOX2

Correspondence: Yoshihiko Hirohashi, MD, PhD, Department of Pathology, Sapporo Medical University School of Medicine, South-1 West-17, Chuo-Ku, Sapporo 060-8556, Japan. Email: hirohash@sapmed.ac.jp

Received 3 March 2012. Accepted for publication 9 July 2012.

Oral squamous cell carcinoma (OSCC) consistently ranks as one of the 10 most frequently diagnosed cancers worldwide.[1] High cure rates can be achieved by either surgery or definitive irradiation in early stage of OSCC, and both speech and swallowing functions can be preserved. Intensive treatments such as a combination of surgical treatment and other adjuvant therapies, such as chemotherapy and radiotherapy, are needed in advanced OSCC cases. Even after intensive treatments, most patients are at high risk for locoregional recurrence and distant metastasis, and poor prognosis.[2] Therefore, identification of factors predicting metastasis of OSCC is necessary.

Cancer cells in solid carcinomas display heterogeneity in many aspects of their phenotypes, and only a small population of cells, known as cancer stem-like cells/cancer-initiating cells (CSCs/CICs), express a stem cell phenotype and have higher tumor-initiating ability (cancer stem cell hypothesis).[3,4] The CSCs/CICs are highly metastatic cells and are thought to be responsible for metastasis. Thus, detection of CSCs/CICs in cancer tissues might be a reasonable approach to predicting metastasis.

Aldehyde dehydrogenase 1 (ALDH1) and SRY-related HMG-box gene 2 (SOX2) have recently been shown to be putative CSC/CIC markers in several malignancies.[5–7] In the present study, we investigated the correlations of expression of ALDH1, SOX2 and Ki67, which is a representative cell proliferation marker, with lymph node (LN) metastasis of OSCC. We found that a high expression rate of ALDH1 is correlated with lymph node metastasis. The staining pattern of SOX2 could be classified into two groups: (i) diffuse staining pattern; and (ii) peripheral staining pattern. The SOX2 diffuse staining pattern was correlated significantly with lymph node metastasis. Therefore, high expression rates of ALDH1 and

SOX2 diffuse staining patterns might be novel prediction markers for lymph node metastasis of OSCC.

MATERIALS AND METHODS

Patients and oral tumor tissues

Tumor tissue samples were collected after obtaining informed consent from 80 primary OSCC patients who underwent surgery for oral cancer at the Department of Oral Surgery, Sapporo Medical University School of Medicine. Detailed clinical data of the patients are summarized in Table 1. Tumor tissues were fixed in 10% buffered formalin and embedded in paraffin.

Immunohistochemical staining

Immunohistochemical staining was performed with formalin-fixed paraffin-embedded sections of surgically resected tumor specimens of OSCC as described previously.[7] For detection of ALDH1, a mouse monoclonal antibody (mAb) specific for human ALDH1 (clone: 44/ALDH, BD Pharmingen) was used at 250-times dilution. Anti-SOX2 (Invitrogen) polyclonal antibodies were used at 400-times dilution. Anti-Ki67 monoclonal antibody (clone: MIB-1, DAKO) was used at 100-times dilution. The positive rates of ALDH1 and Ki67 were the average of positive rates in 10 high power fields. Immunohistochemical staining of ALDH1 was classified as high staining (≥2% positive rates) and low staining (<2% positive rates). SOX2 was classified as peripheral staining pattern (SOX2-positive carcinoma cells being observed within the outer three cancer cell layers of tumor nests) and diffuse staining pattern (SOX2-positive carcinoma cells being observed in more than the outer three layers of tumor nests). Ki67 was classified as high staining (≥30% positive rates) and low staining (<30% positive rates).

Table 1 Clinicopathologic factors in 80 patients with oral squamous cell carcinoma (OSCC)

	No. of cases
Gender	
Male	42
Female	38
Age	
≦65 years	41
>65 years	39
Primary	
Tongue	39
Maxillary gingiva	13
Mandibular gingiva	10
Oral floor	9
Buccal mucosa	4
Hard plate	3
Soft plate	1
Lower lip	1
T status	
T1	19
T2	39
T3	12
T4	10
N status	
N0	55
N1	11
N2a	1
N2b	8
N2c	5
N3	0
Histopathologic grade	
Well	39
Moderate	35
Poor	6

Statistical analysis

Statistical analysis between two groups was performed by the chi square test using the JMP 7 software program (JMP 7.0.1 for Windows; SAS Institute Inc., Cary, NC, USA).

RESULTS

High rate of lymph node metastasis in patients with poorly differentiated SCC

The patients' clinicopathologic factors are summarized in Table 1. All patients were diagnosed with oral squamous cell carcinoma (OSCC) and the carcinomas were classified into three histological grades (well-differentiated SCC, moderately differentiated SCC and poorly differentiated SCC) according to World Health Organization (WHO) classifications (Supplemental Fig. S1).[8] Three histological grades were analyzed for correlation with lymph node metastasis, and only poorly differentiated squamous cell carcinoma showed a significant correlation with lymph node metastasis (5 of 6 cases) compared with well differentiated SCC and moderately differentiated SCC (7 of 39 cases and 13 of 35 cases, respectively) ($P = 0.002$).

Expression of ALDH1 and SOX2 in normal oral squamous cell epitheila

To investigate stem cell marker expression in normal oral squamous cell epithelia, we stained oral mucosa sections with anti-ALDH1 antibody, anti-SOX2 antibody and anti-Ki67 antibodies. No ALDH1 staining was observed in normal squamous cell epithelia. SOX2-positive staining was observed in the two to three bottom layers of squamous cell epithelia

Figure 1 Immunohistological staining of aldehyde dehydrogenase isoform 1 (ALDH1) and SRY-related HMG-box gene 2 (SOX2) in oral squamous cell carcinoma (OSCC) cases. (**a**) ALDH1 staining in OSCC cases. OSCC cases were stained by anti-ALDH1 monoclonal antibody (clone: 44/ALDH). Representative pictures are shown. The ALDH1 positive rates are 0%, 7%, 9% and 19%, respectively. Arrows indicate ALDH1-positive squamous cell carcinoma cells. Scale bars represent 50 μm. Magnification, ×400. (**b**) SOX2 staining in OSCC cases. OSCC cases were stained by anti-SOX2 polyclonal antibody. Left panel is 'SOX2 peripheral staining pattern', and right panel is 'SOX2 diffuse staining pattern'. P indicates SOX2 positive staining area surrounded by solid lines. N indicates SOX2 negative staining area surrounded by a dotted line. In SOX2 peripheral staining pattern case, SOX2 negative staining area is surrounded by SOX2 positive staining area, whereas no SOX2 negative staining area can be observed in SOX2 diffuse staining pattern case. Scale bars represent 50 μm. Magnification, ×400. (**c**) ALDH1 and SOX2 staining in LN metastasis case. Left panel indicate ALDH1 staining (ALDH1 positive rate = 0.5%) and SOX2 staining (SOX2 peripheral staining pattern) of OSCC primary lesion, and right panel indicate ALDH1 staining (ALDH1 positive rate = 2%) and SOX2 staining (SOX2 diffuse staining pattern) in corresponding OSCC LN metastasis lesion. and SOX2 staining Scale bars represent 50 μm. Magnification, ×400. (**d**) ALDH1 expression in OSCC primary lesion and LN metastasis lesion. ALDH1 positive rates in OSCC primary lesion and corresponding LN metastasis lesion are shown. Each line indicate individual case. The average of ALDH1 positive rate in primary lesion and LN metastasis lesion are 2.81% and 7.25%, respectively. The difference in positive rates of primary lesion and LN metastasis lesion is significant ($P = 0.044$). (**e**) SOX2 expression in OSCC primary lesion and LN metastasis lesion. SOX2 staining pattern in in OSCC primary lesion and corresponding LN metastasis lesion are shown. Each line indicate individual case.

(Supplemental Fig. S2). Ki67-positive staining was observed in squamous cells close to the basal layer, which might represent highly proliferating progenitor cells. These observations indicate that normal squamous stem cells and progenitor cells express SOX2.

Correlation of CSC/CIC marker expression with lymph node metastasis

To investigate correlations of CSC/CIC marker expression with tumor progression and lymph node metastasis, we stained sections of the 80 OSCC cases with anti-ALDH1, SOX2 and Ki67 antibodies. ALDH1 staining was observed in the cytoplasm of carcinoma cells (Fig. 1a, Supplemental Fig. S3). The positive rate of ALDH1 expression ranged from 0% to 40%, and the median was 2%. We therefore classified ALDH1 expression into two groups: (i) low ALDH1 group (<2%); and (ii) high ALDH1 group (2–40% staining). A high ALDH1 positive rate was correlated with high histological grade ($P < 0.001$) and with lymph node metastasis ($P = 0.0017$). The high ALDH1 group showed a tendency towards high tumor grade, however, the difference was not significant ($P = 0.086$) (Table 2).

SOX2-positive staining was observed in all cases of OSCC, and we found that the SOX2-positive staining pattern could be classified into two groups: (i) diffuse staining pattern (SOX2-positive carcinoma cells being observed in more than the outer three layers of tumor nests); and (ii) peripheral staining pattern (SOX2-positive carcinoma cells being observed within the outer three cancer cell layers of tumor nests) (Fig. 1b, left panel: peripheral staining pattern, right panel: diffuse staining pattern). In cases of diffuse staining pattern, SOX2-positive staining was observed at relative high intensity in the nucleus. Less intense cytoplasmic staining was observed in some cases. A SOX2 diffuse staining pattern was correlated with lymph node metastasis ($P < 0.001$) and high histological grade ($P < 0.001$) (Table 2).

High expression rates of ALDH1 and SOX2 diffuse staining pattern were correlated with lymph node metastasis, and we compared these with Ki67 staining, which is a representative cell proliferation marker. Ki67-positive rates ranged from 5% to 70% (median = 30%), and we classified Ki67 expression into a high Ki67 group (30%–70%) and a low Ki67 group (<30%). A high Ki67 positive rate showed a correlation with high histological grade but not with tumor grade or lymph node metastasis (Table 2).

ALDH1 expression was upregulated in LN metastasis lesion compared with primary lesion

High expression rates of ALDH1 and diffuse staining pattern of SOX2 were correlated with LN metastasis. Thus, the ALDH1 expression rates and SOX2 staining pattern were compared with primary lesion and LN metastasis lesion in eight OSCC cases. Representative pictures of ALDH1 and SOX2 staining in primary and LN metastasis lesions are shown in Fig. 1c. The average of ALDH1 positive rates in primary lesion of the eight OSCC cases was 2.81%, whereas the average of ALDH1 positive rates in corresponding LN metastasis lesion was 7.25%, and the difference showed statistical significance ($P = 0.044$, Fig. 1d). The SOX2 diffuse staining pattern could be observed in five out of eight primary lesions, whereas SOX2 diffuse staining pattern could be observed in eight out of eight LN metastasis lesions; however, the difference was not statistically significant ($P = 0.079$, Fig. 1e).

DISCUSSION

In this study, we investigated the association of ALDH1 and SOX2 expression with metastasis of OSCC and we showed, for the first time, that expression of ALDH1 was associated with lymph node metastasis in OSCC cases. We also

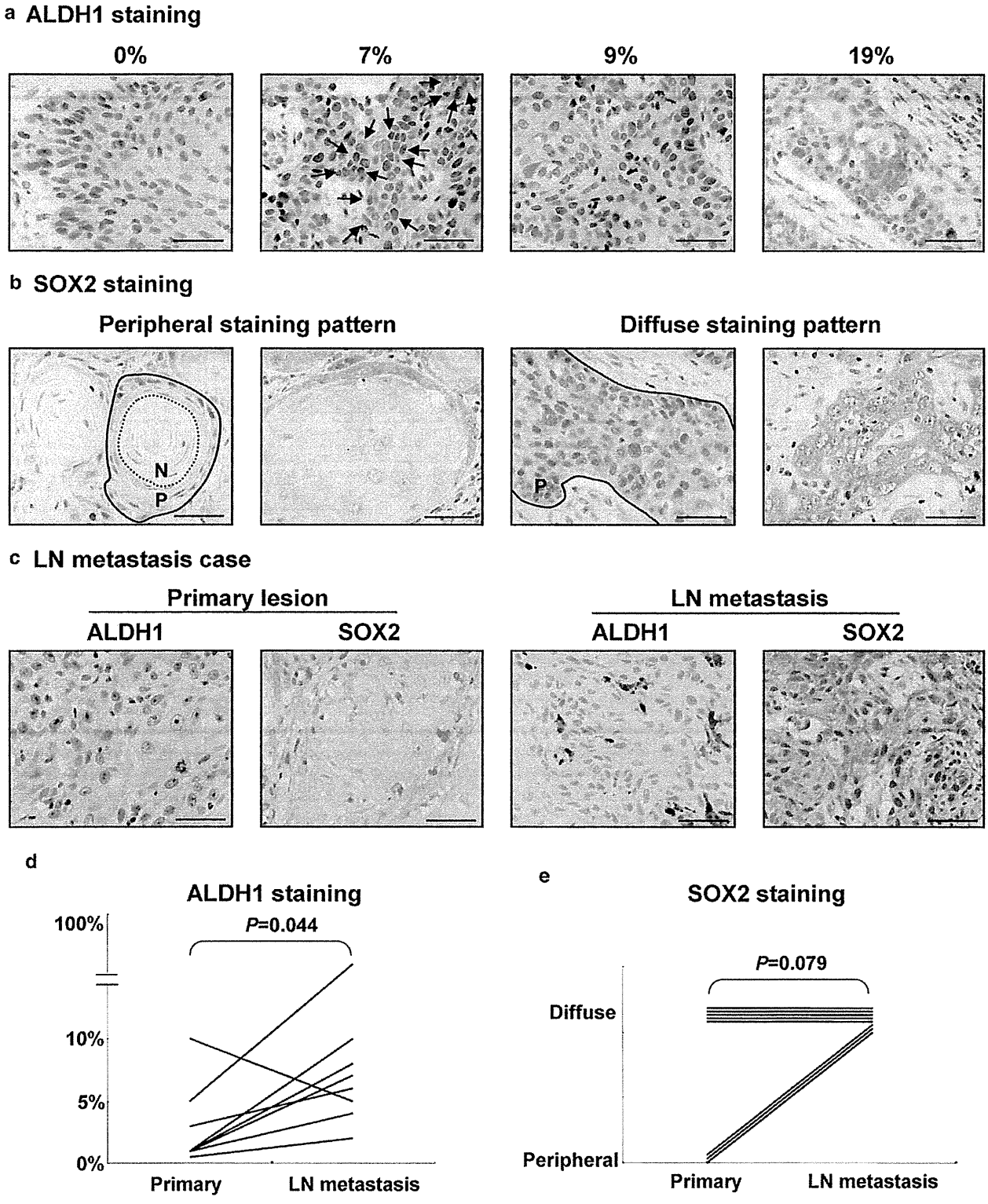

Table 2 Association of cancer stem cell (CSC) marker staining with clinicopathologic feature of oral squamous cell carcinoma (OSCC)

	ALDH1		SOX2		Ki-67	
Total	40/80 (50%)		34/80 (43%)		40/80 (50%)	
% positive cell or staining pattern	2–40%		diffuse staining pattern		30–90%	
Characters	High positive cases (%)	*P* value	diffuse staining pattern cases (%)	*P* value	High positive cases (%)	*P* value
T grade						
T1 and T2	29/65 (43%)	0.086	25/65 (38%)	0.218	31/65 (48%)	0.567
T3 and T4	11/15 (73%)		9/15 (60%)		9/15 (60%)	
N grade						
N0	21/55 (38%)	0.0017	16/55 (29%)	<0.001	31/55 (56%)	0.148
N1/2	19/25 (76%)		18/25 (72%)		9/25 (36%)	
Histology						
Well	7/39 (18%)	<0.001	2/39 (5%)	<0.001	13/39 (33%)	0.019
Moderate	26/35 (74%)		27/35 (77%)		24/35 (69%)	
Poorly	6/6 (100%)		5/6 (83%)		3/6 (50%)	

showed that the SOX2 staining could be classified into two patterns (diffuse staining pattern and peripheral staining pattern) and that the SOX2 diffuse staining pattern was associated with lymph node metastasis of OSCC.

The aldehyde dehydrogenase (ALDH) family of enzymes are cytosolic isoenzymes that are responsible for oxidizing intracellular aldehydes and contributing to the oxidation of retinol to retinoic acid in early stem cell differentiation.[9] High ALDH1 activity has been used to isolate normal hematopoietic stem cells.[10,11] In the following works, CSCs/CICs of breast carcinomas were successfully isolated by using ALDH1 activity.[5] We have shown along with Chen *et al.* that ALDH1 is a CSC/CIC marker and that its presence strongly correlates with tumor malignancy as well as self-renewal properties of stem cells in HNSCC (unpublished data).[12] We have also shown that ALDH1-positive prostate CSCs/CICs have grater invasion capability than that of the ALDH1-negative population.[13] Therefore, ALDH1-positive putative CSCs/CICs have high cancer-initiating ability and also have high invasion ability, and these properties might be related to lymph node metastasis.

SOX2, a member of the SOX (SRY-related HMG-box gene) family, was originally discovered as a gene involved in the maintenance of embryonic stem cell pluripotency.[14,15] SOX2 has recently been found to serve as a link of malignancy and 'stemness' and as a prognostic factor in different types of tumors.[16,17] SOX2 expression has been shown to be involved in tumor progression in lymph node metastasis-negative oral tongue squamous cell carcinomas.[18] These observations indicate that high rates of CSCs/CICs are related to disease progression and prognosis. In this study, we observed SOX2-positive staining in almost all cases; however, the staining pattern could be classified into two groups. We used a different antibody from the monoclonal antibody that Du *et al.* used for staining of tongue squamous cell carcinoma cases. The difference in antibodies might result the difference in staining pattern of SOX2 in OSCC cases. Since SOX2 is expressed in the two or three bottom layers of normal squamous epithelia, SOX2 might be expressed in normal squamous stem cells and progenitor cells. Therefore, the SOX2 diffuse staining pattern might indicate a 'loss of differentiation', whereas SOX2 peripheral staining pattern might indicate 'differentiation'. Also, the loss of differentiation might be related to high rates of LN metastasis. In cases of diffuse staining pattern, SOX2 positive staining was observed at higher intensity in the nucleus compared with peripheral staining pattern. Thus, the SOX2 diffuse staining pattern might be related to the higher nuclear staining that Du *et al.* described, and SOX2 diffuse staining patterns are related to lymph node metastasis.

In summary, we showed for the first time that a high rates of ALDH1-positive staining and SOX2 diffuse staining pattern were related to lymph node metastasis of OSCC cases. These CSC/CIC marker staining might be useful for lymph node metastasis prediction.

ACKNOWLEDGMENTS

This work was supported by Grants-in-Aid for Scientific Research from the Ministry of Education, Culture, Sports, Science and Technology of Japan (grant nos. 16209013, 17016061 and 15659097) for Practical Application Research from the Japan Science and Technology Agency, and for Cancer Research (15–17 and 19-14) from the Ministry of Health, Labor and Welfare of Japan, Ono Cancer Research Fund (to N. S.) and Takeda Science Foundation (to Y. H.). This work was supported in part by the National Cancer Center Research and Development Fund (23-A-44).

REFERENCES

1 Rodrigues VC, Moss SM, Tuomainen H. Oral cancer in the UK: To screen or not to screen. *Oral Oncol* 1998; **34**: 454–65.

2 Yao M, Epstein JB, Modi BJ, Pytynia KB, Mundt AJ, Feldman LE. Current surgical treatment of squamous cell carcinoma of the head and neck. *Oral Oncol* 2007; **43**: 213–23.
3 Park CY, Tseng D, Weissman IL. Cancer stem cell-directed therapies: Recent data from the laboratory and clinic. *Mol Ther* 2009; **17**: 219–30.
4 Hirohashi Y, Torigoe T, Inoda S *et al.* Immune response against tumor antigens expressed on human cancer stem-like cells/tumor-initiating cells. *Immunotherapy* 2010; **2**: 201–11.
5 Ginestier C, Hur MH, Charafe-Jauffret E *et al.* ALDH1 is a marker of normal and malignant human mammary stem cells and a predictor of poor clinical outcome. *Cell Stem Cell* 2007; **1**: 555–67.
6 Chen Y, Shi L, Zhang L *et al.* The molecular mechanism governing the oncogenic potential of SOX2 in breast cancer. *J Biol Chem* 2008; **283**: 17969–78.
7 Nakatsugawa M, Takahashi A, Hirohashi Y *et al.* SOX2 is overexpressed in stem-like cells of human lung adenocarcinoma and augments the tumorigenicity. *Lab Invest* 2011; **91**: 1796–804.
8 Barnes L, Eveson J, Reichart P, Sidransky D. *WHO Classification Head and Neck.* IARC, Geneva, 2005.
9 Yoshida A. Molecular genetics of human aldehyde dehydrogenase. *Pharmacogenetics* 1992; **2**: 139–47.
10 Armstrong L, Stojkovic M, Dimmick I *et al.* Phenotypic characterization of murine primitive hematopoietic progenitor cells isolated on basis of aldehyde dehydrogenase activity. *Stem Cells* 2004; **22**: 1142–51.
11 Hess DA, Wirthlin L, Craft TP *et al.* Selection based on CD133 and high aldehyde dehydrogenase activity isolates long-term reconstituting human hematopoietic stem cells. *Blood* 2006; **107**: 2162–9.
12 Chen YC, Chen YW, Hsu HS *et al.* Aldehyde dehydrogenase 1 is a putative marker for cancer stem cells in head and neck squamous cancer. *Biochem Biophys Res Commun* 2009; **385**: 307–13.
13 Nishida S, Hirohashi Y, Torigoe T *et al.* Gene expression profiles of prostate cancer stem cells isolated by ALDH activity assay. *J Urol* 2012; **188**: 294–9.
14 Ivanova N, Dobrin R, Lu R *et al.* Dissecting self-renewal in stem cells with RNA interference. *Nature* 2006; **442**: 533–8.
15 Wang J, Rao S, Chu J *et al.* A protein interaction network for pluripotency of embryonic stem cells. *Nature* 2006; **444**: 364–8.
16 Bass AJ, Watanabe H, Mermel CH *et al.* SOX2 is an amplified lineage-survival oncogene in lung and esophageal squamous cell carcinomas. *Nat Genet* 2009; **41**: 1238–42.
17 Freier K, Knoepfle K, Flechtenmacher C *et al.* Recurrent copy number gain of transcription factor SOX2 and corresponding high protein expression in oral squamous cell carcinoma. *Genes Chromosomes Cancer* 2010; **49**: 9–16.
18 Du L, Yang Y, Xiao X *et al.* Sox2 nuclear expression is closely associated with poor prognosis in patients with histologically node-negative oral tongue squamous cell carcinoma. *Oral Oncol* 2011; **47**: 709–13.

SUPPORTING INFORMATION

Additional Supporting Information may be found in the online version of this article:

Figure S1. Histological grading of oral squamous cell carcinomas. Representative images of well-differentiated, moderately differentiated and poorly differentiated squamous cell carcinomas. Magnification, ×40.

Figure S2. Expression of ALDH1, SOX2 and Ki67 in human normal oral mucosa. Magnification, ×40 (left panel), ×200 (right panel).

Figure S3. Expression of ALDH1, SOX2 and Ki67 in human oral carcinomas. Representative ALDH1 low case (0%, left panel) and ALDH1 high case (30%, right panel), SOX2 peripheral staining pattern (left panel) and SOX2 diffuse staining pattern (right panel), and Ki67 low case (3%, left panel) and Ki67 high case (60%, right panel) are shown. Magnification × 40.

Please note: Wiley-Blackwell are not responsible for the content or functionality of any supporting materials supplied by the authors. Any queries (other than missing material) should be directed to the corresponding author for the article.

Experimental and Molecular Pathology 92 (2012) 185–190

Contents lists available at SciVerse ScienceDirect

Experimental and Molecular Pathology

journal homepage: www.elsevier.com/locate/yexmp

Novel oligomannose liposome-DNA complex DNA vaccination efficiently evokes anti-HPV E6 and E7 CTL responses

Masahito Mizuuchi [a,b], Yoshihiko Hirohashi [a,*], Toshihiko Torigoe [a,*], Takafumi Kuroda [a,b], Kazuyo Yasuda [a], Yoshitaka Shimizu [c], Tsuyoshi Saito [b], Noriyuki Sato [a]

[a] Department of Pathology, Sapporo Medical University School of Medicine, South-1 West-17, Chuo-Ku, Sapporo 060-8556, Japan
[b] Department of Obstetrics and Gynecology, Sapporo Medical University School of Medicine, South-1 West-17, Chuo-Ku, Sapporo 060-8556, Japan
[c] BioMedCore Inc., Hanasakicho 5-136-5-601, Nishi-Ku, Yokohama 220-0022, Japan

ARTICLE INFO

Article history:
Received 29 September 2011
Available online 14 October 2011

Keywords:
HPV
CTL
HLA-A24
E6
E7
Oligomannose-coated liposome

ABSTRACT

The aim of this study was to establish an efficient human papilloma virus (HPV) type 16-targeting cancer immunotherapy. Persistent high-risk HPV infection causes cervical intra-epithelial neoplasia (CIN) and subsequent cervical carcinoma. HPV type16 (HPV16) is one of the common carcinogenic types and is found in about 50% of invasive cervical carcinomas. HPV16-derived viral proteins E6 and E7 are expressed in cancerous cells through the progression of the disease and have a role in carcinogenesis but are not expressed in normal cells. Thus, these proteins are regarded as ideal antigens for cervical carcinoma immunotherapy. In this study, we generated a novel HPV 16 E6 and E7 gene plasmid containing oligomannose liposomes (OML-HPV). We compared the cytotoxic T lymphocyte (CTL) induction efficiency of OML-HPV and that of standard liposome-HPV16 E6 and E7 DNA complex. HPV16 E6-specific CTLs could be generated from HPV 16-positive cervical carcinoma patient's peripheral blood mononuclear cells (PBMCs) by stimulating OML-HPV, but could not by stimulating standard liposome-HPV 16 E6, E7 DNA complex. Furthermore, we screened HLA-A24-restricted HPV16 E6- and E7-derived peptides, and found that one E6-derived peptide (E6 66–74) showed the highest immunogenicity with ELISPOT assay from 100% of HPV16-positive patients (4 out of 4). On the other hand, other E6- or E7-derived peptides, including E6 49–57, E6 82–90, E6 87–95, E6 98–106 and E7 83–93, showed less frequent reactivity. These results indicate that OML-HPV is a more effective approach than DNA vaccination using standard liposomes, and that a novel HLA-A24-restricted peptide, E6 66–74, might be a suitable target of cervical cancer immunotherapy.

Introduction

Cervical carcinoma is the second most frequent gynecological malignancy in the world. Cervical cancer and pre-malignant cervical intraepithelial neoplasia (CIN3) are caused by persistent infection with high-risk human papillomavirus (HPV). HPVs are classified into low- and high-risk subtypes, and high-risk types of HPVs are associated with CIN and cervical cancer, while low-risk HPVs are associated with genital warts. The International Agency for Research on Cancer (IARC) classified as HPV types 16, 18, 31, 33, 35, 39, 45, 51, 52, 56, 58, 59, 68, 73 and 82 as high-risk HPV (oncogenic HPV) (Muñoz et al., 2003). The distributions of HPV serotypes differ depending on the region. In Asia, especially in Japan, 21 serotypes of high-risk HPV have been detected in cervical cancer patients. Worldwide, HPV16 and 18 are the most common serotypes and have been found in over 70% of cases. HPV has a circular, double-stranded DNA genome that is approximately 7.9 kb in size and encodes eight genes, in which L1 and L2 are structural proteins and E1 has the function of viral DNA replication, E2 regulates viral transcription, E4 function is unknown, and E5, E6 and E7 have transforming properties (zur Hausen, 2002).

E6 and E7 viral oncogenes interact synergistically with each for progression of cervical cancer. E5, E6 and E7 are expressed only in CIN3 and cervical carcinomas and can be ideally used as therapeutic vaccines (Hirohashi et al., 2009; Roden et al., 2004). Following primary infection with HPV virus, development of advanced cervical cancer needs between 15 and 25 years, and expression of E6 and E7 oncogenes can be detected through the course of development of the disease.

A prophylactic HPV vaccine that effectively prevents persistent HPV infection and associated disease by the induction of neutralizing antibodies against the envelope proteins of HPV16 and HPV18 is currently on the market in the USA (Pallecaros and Vonau, 2007).

Abbreviations: HPV, human papillomavirus; CTL, cytotoxic T lymphocyte; OML, oligomannose-coated liposome; CIN, intraepithelial neoplasia; PBMC, peripheral blood mononuclear cell.

* Corresponding authors. Fax: +81 11 643 2310.
E-mail addresses: hirohash@sapmed.ac.jp (Y. Hirohashi), torigoe@sapmed.ac.jp (T. Torigoe).

0014-4800/$ – see front matter © 2011 Elsevier Inc. All rights reserved.
doi:10.1016/j.yexmp.2011.10.002

Although this vaccine is very efficient for prevention of persistent infection by HPV16 and HPV18 following CIN and carcinomas, there is no evidence for its efficacy against established HPV16 and HPV18 genital lesions. A therapeutic vaccine is still needed because an estimated 5 million deaths from cervical cancer will occur in the next 20 years due to existing HPV infections.

DNA vaccine is one of major methods to achieve antigen-specific T cell immune response. Recently, a liposome coated with a neoglycolipid constructed from mannotriose and dipalmitoylphosphatidylethanolamine (Man3-DPPE) that activates macrophages to induce enhanced expression of co-stimulatory molecules and MHC class II has been reported and it might be useful for a DNA vaccine as an adjuvant for efficient DNA vaccine therapy (Ikehara et al., 2008).

In this study, we generated OML-coated HPV16 E6 and E7 plasmid DNA (OML-HPV) to target the viral proteins E6 and E7. OML-HPV could generate anti-E6- and E7-specific immunological reactivity, and the CTL induction was more efficient than that by a standard liposome. We identified novel HLA-A*2402-restricted HPV16 E6 66–74 and E7 83–93 epitopes with the CTLs induced by OML-HPV, and E6 66–74 antigenic peptide was found to be the most immunogenic peptide within the HLA-A24-restricted peptides that were tested. These observations suggest that OML-coated HPV DNA might be an efficient means to generate anti-HPV-specific CTLs and also suggest that E6 66–74 peptide is one of the most immunogenic peptides of HLA-A24-restricted E6-coded peptides. Thus, OML-HPV DNA vaccine and E6 66–74 antigenic peptide might provide a more efficient way to immunize patients with HPV16-positive CIN3 or cervical carcinoma.

Materials and methods

Blood donors and cervical cytology samples

Twenty-nine HLA-A*2402-positive patients who had been diagnosed with CIN3 or invasive cervical carcinoma histologically at the Department of Gynecology, Sapporo Medical University Hospital were enrolled this study. Informed consent was obtained from all patients. Cervical cytology was also performed to detect HPVs. HPV genotyping was performed at GLab Pathology Center (Sapporo, Japan) with the multiplex PCR method. HLA-A24 genotyping by PCR-SSP was performed as described previously (Nakatsugawa et al., 2011).

Cells and cytokine

T2-A*2402, a stable transfectant of HLA-A*2402 cDNA of T2 cells (a kind gift from Dr. K. Kuzushima, Aichi Cancer Research Institute), was cultured in RPMI 1640 supplemented with 10% fetal bovine serum and 0.8 μg/mL G418 (Invitrogen). 293T human embryonic kidney cells were cultured in DMEM (SIGMA, St. Louis, MO) supplemented with 10% fetal bovine serum. Human recombinant IL-2 was a kind gift from Takeda Pharmaceutical (Osaka, Japan).

Synthetic peptides

To determine a potential vaccine candidate, nine peptides, HPV16-E6 8–19 (MFQDPQERPRKL), HPV16-E6 49–57 (VYDFAFRDL), HPV16-E6 66–74 (PYAVCDKCL), HPV16-E6 82–90 (EYRHYCYSL), HPV16-E6 87–95 (CYSLYGTTL), HPV16-E6 98–106 (QYNKPLCDL), HPV16-E7 10–20 (IVLHLEPQNEI), HPV16-E7 51–60 (HYNIVTFCCK) and HPV16-E7 83–93 (LMGTLGIVCPI), were derived from the amino acid sequence of HPV16-E6 or HPV16-E7 based on the HLA-A24-binding motifs (Table 1). An HLA-A24-restricted EBV LMP2-derived peptide (TYGPVFMSL) and an HIV env-derived peptide (RYLRDQQLLGI) were used as positive controls for the HLA-A24 binding assay. An H2-Kd-restricted Ovalbumin (OVA)-derived SL-8 peptide (SIINFEKL) and an HLA-A68-restricted EBV peptide (FTASVSTVV) (Straathof et al., 2005) were used as negative controls for the HLA-A24 binding assay. All peptides were synthesized at and purchased from Sigma Genosis (Ishikari, Hokkaido, Japan). Peptides were dissolved in DMSO and stored at −80 °C before use.

Table 1
Summary of HLA-A24 binding motif-positive HPV16 E6 and E7 derived peptides.

Gene	Position	Peptides	Sequences	BIMAS score
E6	8–19	E6 8–19	MFQDPQERPRKL	n.d.[a]
E6	49–57	E6 49–57	VYDFAFRDL	240
E6	66–74	E6 66–74	PYAVCDKCL	20
E6	82–90	E6 82–90	EYRHYCYSL	200
E6	87–95	E6 87–95	CYSLYGTTL	200
E6	98–106	E6 98–106	QYNKPLCDL	300
E7	10–20	E7 10–20	IVLHLEPQNEI	n.d.[a]
E7	51–60	E7 51–60	HYNIVTFCCK	0.9
E7	83–93	E7 83–93	LMGTLGIVCPI	n.d.[a]

[a] BIMAS web site shows the peptide binding score with only 9- and 10-mer peptides.

Peptide binding assay

Peptide binding affinity to HLA-A24 molecules was assessed by an HLA-A24 stabilization assay as described previously (Nakao et al., 2000) based on the finding that MHC class I molecules could be stabilized on the cell surface in the presence of binding peptides. T2-A*2402 cells are the transporter associated with an antigen processing (TAP)-negative cell line transfected with a plasmid coding HLA-A*2402. After incubation of T2-A*2402 cells in culture medium at 26 °C for 18 h, 2×10^5 cells were washed with PBS and suspended with 1 mL Opti-MEM (Invitrogen) with or without 100 μg peptide followed by incubation at 26 °C for 3 h and then at 37 °C for 2.5 h. After washing with ice-cold PBS, the cells were incubated with anti-HLA-A24 monoclonal antibody at 4 °C for 1 h followed by incubation with FITC-conjugated rabbit anti-mouse IgG at 4 °C for 30 min. The cells were then suspended with 1 mL PBS containing 1% formaldehyde and analyzed by a FACS caliber (Becton Dickinson). Binding affinity was evaluated by comparing mean fluorescence intensity (MFI).

Construction of HPV16 E6E7 fusion gene expression plasmids and preparation of oligomannose-coated liposomes (OMLs)

A FLAG-tagged HPV16E6 and E7 fused gene was subcloned into pcDNA3.1 expression vector (Invitrogen). E6 and E7 genes were amplified from cDNA of a Caski HPV16-positive cervical carcinoma cell line. Primer pairs used for RT-PCR are 5′-CGCGAATTCTGCCACCATGCACCAAAAGAGAACTGCA-3′ and 5′-CGCGATATCCAGCTGGGTTTCTCTATGGAA-3′ for E6 and 5′-CGCGATATCGCCACCATGCATGGAGATACACCTACA-3′ and 5′-ATAAGAATGCGGCCGCCTGGTTTCTGGGAACAGATGGG-3′ for E7. The purified PCR product was digested with *EcoRI* and *EcoRV* restriction enzymes for E6 and with *EcoRV* and *NotI* restriction enzymes for E7 and then each product was ligated into the digested pcDNA3.1 plasmid. The sequence of the cDNA was confirmed with an ABI Genetic analyzer PRIM 3100 (PerkinElmer). Then the FLAG-tag fused E6E7 gene was subcloned into pCAGGS expression vector (kind gift from Dr. Miyazaki J, Osaka, Japan (Miyazaki et al., 1989)).

Procedures for plasmid-encasing of oligomannose-coated liposomes (OMLs) were performed as described previously (Ikehara et al., 2006).

Western blot analysis

Cultured cells were washed in ice-cold PBS and lysed by incubation on ice in a lysis buffer (50 mmol/L Tris–HCl [pH 8.0], 150 mmol/L NaCl, 1% NP40, protease inhibitor cocktail; Complete, Roche Diagnostics, Inc., Basel, Switzerland). The whole-cell lysates were resolved by 12% SDS-PAGE and electrophoretically transferred to nitrocellulose membranes (BIO-RAD). After blocking with 5% nonfat dry milk, the membranes were incubated with the anti-FLAG mAb